POLITECNICO DI TORINO

Master's Degree in Civil Engineering

Master thesis:

Small-scale flume modelling of the interaction between dry granular flow and deflecting dams

Supervisors:

Prof. Marina Pirulli

Prof. Claudio Scavia

Prof. Alessandro Leonardi

Candidate:

Filippo Mauro

Academic Year 2018/2019

Abstract

Debris flow mixture may be composed by coarse and fine soil, water, and rock boulders in various uncertain concentrations, and they represent a threat whose complex mechanism requires further understanding. This work focuses on the ideal composition of pure sandy flow, and is intended to study the interaction of a dry granular flow with obstacles on its path. Typical protection measures against material flows are deflecting dams, which are rigid structures meant to direct the flow far from inhabited areas and infrastructures. Previous works analysed the mechanism of interaction and provided design criteria to choose the dam height, based on single particle mass, centre-of-mass model, and oblique shock theory.

In this study, a small-scale flume is used to realise a physical model of channelised granular flow. Several experiments are carried out in order to comprehend the interaction between a sand flow and a mitigation system composed by two dams, one on each side of the channel. By keeping constant the longitudinal position of one of the two dams, the deflecting system is totally defined by three geometrical parameters. The angle θ represents the inclination of the dam with respect to the flow direction, the spacing d is the longitudinal distance between the position of the two dams, and the aperture a is the space between the obstacles in the direction orthogonal to the flow path. Data about retained mass and residual depth by the dam indicate that the geometry does not affect significantly the retaining capability of this system, at least not in those configurations. The peak depth obtained by the dam can reach even 4.5 times the undisturbed peak flow depth. In case of aperture $a \neq 0$, the front is reduced in width, but it is not slowed down. On the contrary, a substantial dissipation of momentum is observed if $a = 0$.

Contents

1. Introduction

Landslides of the flow type are mountainous phenomena which are not new to put in real danger human lives, goods and infrastructures. Protective barriers are usually adopted in order to stop, or at least mitigate, the disruptive free-surface gravity-driven flows. To prevent against those flows, potentially presenting high values of kinetic energy, a typical protective measure is represented by the deflecting dams. Dams are rigid walls with the purpose of screening an area at risk by diverting the mass towards non-populated zones. In this process, it is important to avoid the overflow phenomenon, in order to control the potentially threatened area. Theoretical models were proposed to design a deflecting dam, from the traditional simple point mass criterion (Jóhannesson 2001) to a model based on momentum equations (Jóhannesson 2009). Previous works have been addressed to the fundamental mechanism of incidence between snow avalanches and a single deflecting dam (Domaas and Harbitz 1998, Hákonardóttir and Hogg 2005, Cui et al. 2007).

State-of-the-art solutions for protection against debris flows are indeed needed. This project started from the initial idea of developing new flexible nets capable to self-clean over time. The concept was borrowed from the spur dykes realised on the riversides. Those spurs contrast the erosion of the riverbed by retaining the solid material carried downstream by the river flow. As first experimentation, it is chosen to address the study to simple physical models, constituted by rigid structures, which guarantee easy setup and repeatability. This project develops the physical modelling of a deflecting system, constituted by two dams. Under the hypothesis of channelised flow, a small-scale flume is assembled with one dam per side, and instrumented with cameras to record the flow kinematics from the top and the side. The acquired videos are calibrated by square grids marked on the basal and lateral surfaces of the channel. The flow depth distribution along the chute length, the peak flow depth and residual by the dam, and the frontal velocity evolution were observed through video analysis. The objective of this survey is to evaluate the influence of the geometrical parameters defining the deflecting system on the interaction mechanism with a granular flow. The material chosen for the tests was dry Toyoura sand, which is a fairly homogeneous non-cohesive soil with internationally recognised standard properties.

In this work, it is firstly illustrated a classification of landslide phenomena. *Chapter 2* shows especially the differences between various kinds of flow-like movements. In *Chapter 3*, the protection measures are presented, while *Chapter 4* focuses on previous studies about the interaction between granular flows and deflecting dams, which is a particular type of defence structure against mountainous flows. In *Chapter 5*, the physical modelling developed by this study is presented. The experimental results are analysed and discussed in *Chapter 6*. Eventually, conclusions are drawn in *Chapter 7* and further works are proposed.

2. **Landslide phenomena**

The landslide classification of Varnes (1978) is widely accepted in the English-speaking world. However, literature on engineering geology of landslides is continuously affected by inconsistent terminology and ambiguous definitions of different landslide types. Hungr et al. (2001) show that landslide phenomena can be divided into a number of classes, which conserve established concepts and at the same time bring out the most important attributes of landslide events. In the scheme of Varnes (1978), all slope movements involving significant internal distortion of a moving mass would be classed as flows (Table 2.1). In a narrower sense, flow can also be understood as the motion of a fluid material over a rigid bed (Hungr et al. 2001). Varnes (1978) also distinguishes between debris and earth materials based on the percentage content of coarse material. "Earth" has less than 20 percent of gravel and coarser clasts (grain diameter greater than 2 mm) while "debris" has more. Poorly sorted materials can be fully supported by clayey matrix with coarse-grain content as high as 65 percent by volume (Rodine and Johnson 1976). Therefore, the limit of 20 percent content of coarse clasts may have little significance with respect to mechanical behaviour (Hungr et al. 2001).

Rate of Movement	Bedrock	Debris (<80% Sand and Finer)	Earth (>80% Sand and Finer)
rapid and higher (>1.5 m/day)	rock flow (creep, slope sagging)	debris flow debris avalanche	wet sand and silt flow rapid earth flow loess flow dry sand flow
less then rapid (<1.5 m/day)		solifluction soil creep block stream	earth flow

Table 2.1 – Key terms for mass movement in the flow category. (Varnes 1978)

For the purposes of an engineering-geological landslide classification, it may be useful to replace grain-size criteria by genetic concepts. One group may contain sorted fine-grain deposits (sand, silt or clay) produced by fluvial, lacustrine, marine, aeolian or volcanic processes (e.g. ash fall), or sorted anthropogenic deposits (e.g. mine tailings). Flows in such

materials could be referred to using the specific textural or genetic label of the soil involved, such as sand, clay, loess or talus. The presence of sorting is implicit in the geomorphic process responsible for the origin of the deposit. This can be determined by geomorphological techniques in the field, or by remote sensing, without the need to impose arbitrary textural criteria.

The term “earth” is useful in connection with the well-established North American term earth flow (Varnes 1978), which must be distinguished from the equally well-established term debris flow. Earth flow involves the products of weathering of stiff clays and clay-rich rocks such as mudstones, shales and certain metamorphic rocks (Hungr et al. 2001). Weathering produces a clayey colluvium with a consistency closer to the Plastic Limit than the Liquid Limit. Many typical earth flows contain large percentages of gravel and coarser particles, albeit often in a friable form.

However, not all clayey colluvium forms earth flows. Clay slopes under arid climatic conditions produce liquid, extremely rapid debris flows, also referred to as mud flows. Geologically the term mud refers to liquid or semi-liquid clayey material. Rapid mixing of the originally stiff or dry clayey matrix with surface water is required to raise the water content to, or above the Liquid Limit. Debris can be defined as loose unsorted material of low plasticity such as that produced by mass wasting processes (colluvium), weathering (residual soil), glacier transport (till or ice contact deposits), explosive volcanism (granular pyroclastic deposits) or unsorted anthropogenic waste, such as mine spoil. Debris also contain a significant proportion of organic mulch (Swanston 1974).

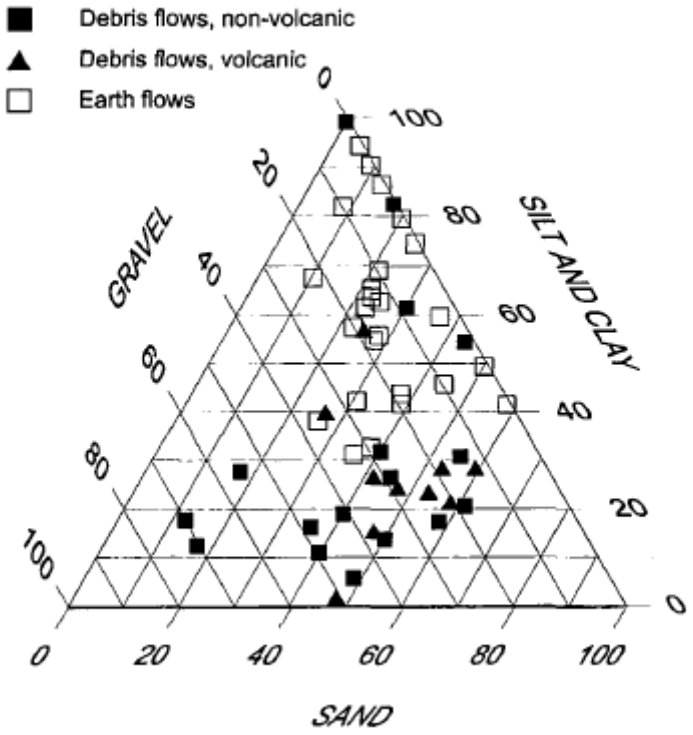

Figure 2.1 – Textural composition of the matrix material in debris flows and earth flows: gravel, 2-18 mm; sand, 0.074-2 mm; silt and clay, < 0.074 mm. (Hungr et al. 2001)

In Figure 2.1, matrix compositions of earth flows, debris flows and mud flows from several areas in the world are compared. Debris typically contain less than 30 percent silt and finer particles. On this basis, they can be distinguished from earth flows. However, mud flows cannot be distinguished from earth flows on a textural basis. Given the situation, the distinction between debris and earth should not be based solely on grain-size distribution, but should instead be derived from the context of each landslide class (Hungr et al. 2001).

Origin	Character	Condition[1]	Name
SORTED (marine, lacustrine, fluvial, eolian, volcanic, anthropogenic)	Non-cohesive P.I. < 5%	Dry or Saturated	- Gravel - Sand - Silt
	Cohesive P.I. > 5%	- Plastic (I_L < 0.5) - Liquid (I_L > 0.5)	- Clay - Sensitive Clay
UNSORTED (residual, colluvial, glacial, volcanic, anthropogenic)	Non-cohesive P.I. < 5%	Dry or Saturated	- Debris[2]
	Cohesive P.I. > 5%	- Plastic (I_L < 0.5) - Liquid (I_L > 0.5)	- Earth - Mud
PEAT	Organic	Saturated	- Peat
ROCK	Fragmented	Dry or Saturated	- Rock

[1] Related to the material found in the vicinity of the rupture surface at the time of failure, if it can be determined. In many cases, the material condition must be deduced from the behavior of the landslide, especially velocity.
[2] Debris may contain a considerable proportion of organic material.

Table 2.2 – Material involved in landslides of the flow type. (Hungr et al. 2001)

A proposed scheme for the classification of materials involved in flows is shown in Table 2.2, as reported by Hungr et al. (2001). The first level of distinction between sorted and unsorted soil and fragmented rock, can be achieved using geomorphological techniques, which can identify the likely character of deposits based on genesis. At the second level, the distinction between cohesive and non-cohesive materials may also be derived from geomorphological analysis, augmented by field observations and, perhaps, laboratory testing. At the third level, the distinctions between saturated versus dry, and liquid versus plastic, can often only be derived inference from the observed landslide behaviour, since the condition of the material in the vicinity of the rupture surface during motion may be very difficult to ascertain. Extremely high velocity and long runout on sloped flatter then the effective dynamic friction angle often signifies the presence of saturation and excess pore pressure.

Hungr et al. (2001) also states that the velocity of landslide movement is a function of time and space ad can rarely be mapped in detail. Reported Velocities are usually random observations at a point at a given moment. However, given the wide spectrum of speeds, such observations are still useful.

In the kinematic category of flows, Varnes (1978) defined 11 key terms, as listed in Table 2.1, among those the most important terms are: *debris flow*, *debris avalanche*, *rapid earth flow* and *earth flow*. New definitions are proposed by Hungr et al. (2001) which do not stray too far from the original meanings imparted by Varnes (1978), but bring out distinctions of practical importance. Hungr et al. (2001) also defined two important landslide types not addressed by Varnes (1978): *mud flow* and *debris flood* are also defined. The term *rock avalanche*, which Varnes (1978) included under "complex landslides", is also considered as it closely related to other phenomena under discussion.

Material	Water Content[1]	Special Condition	Velocity	Name
Silt, Sand, Gravel, Debris (talus)	dry, moist or saturated	- no excess pore-pressure, - limited volume	various	Non-liquefied sand (silt, gravel, debris) flow
Silt, Sand, Debris, Weak rock[2]	saturated at rupture surface content	- liquefiable material[3], - constant water	Ex. Rapid	Sand (silt, debris, rock) flow slide
Sensitive clay	at or above liquid limit	- liquefaction *in situ*,[3] - constant water content[4]	Ex. Rapid	Clay flow slide
Peat	saturated	- excess pore-pressure	Slow to very rapid	Peat flow
Clay or Earth	near plastic limit	- slow movements, - plug flow (sliding)	< Rapid	Earth flow
Debris	saturated	- established channel[5], - increased water content[4]	Ex. Rapid	Debris flow
Mud	at or above liquid limit	-fine-grained debris flow	> Very rapid	Mud flow
Debris	free water present	- flood[6]	Ex. Rapid	Debris flood
Debris	partly or fully saturated	- no established channel[5], - relatively shallow, steep source	Ex. Rapid	Debris avalanche
Fragmented Rock	various, mainly dry	- intact rock at source, - large volume[7]	Ex. Rapid	Rock avalanche

[1] Water content of material in the vicinity of the rupture surface at the time of failure.
[2] Highly porous, weak rock (examples: weak chalk, weathered tuff, pumice).
[3] The presence of full or partial *in situ* liquefaction of the source material of the flow slide may be observed or implied.
[4] Relative to *in situ* source material.
[5] Presence or absence of a defined channel over a large part of the path, and an established deposition landform (fan). Debris flow is a recurrent phenomenon within its path, while debris avalanche is not.
[6] Peak discharge of the same order as that of a major flood or an accidental flood. Significant tractive forces of free flowing water. Presence of floating debris.
[7] Volume greater than 10,000 m^3 approximately. Mass flow, contrasting with fragmental rock fall.

Table 2.3 – Classification of landslides of the flow type. (Hungr et al. 2001)

2.1 **Definitions of landslides of the flow type**

A definition of each class reported in Table 2.3, according to Hungr et al. (2001), is now given.

a) "*Dry (or non-liquefied) sand (silt, gravel or debris) flow* is a flow-like movement of loose dry or moist, sorted or unsorted granular material, without significant excess pore pressure. Dry sand flow is a fundamental process in the migration of sand dunes (Figure 2.2). Unsorted debris of colluvial, volcanic or other origin can also flow in a dry condition. Dry silt flow is sometimes triggered by the collapse of steep silt scarps or cliffs. Non-liquefied saturated sand or gravel flow transports sediment on relatively coarse and steep delta fronts or on channel bottom dunes, with limited mobility. Such relatively small and benign subaqueous mass movements, must be clearly separated from subaqueous debris flows and flow slides (Terzaghi 1957)."

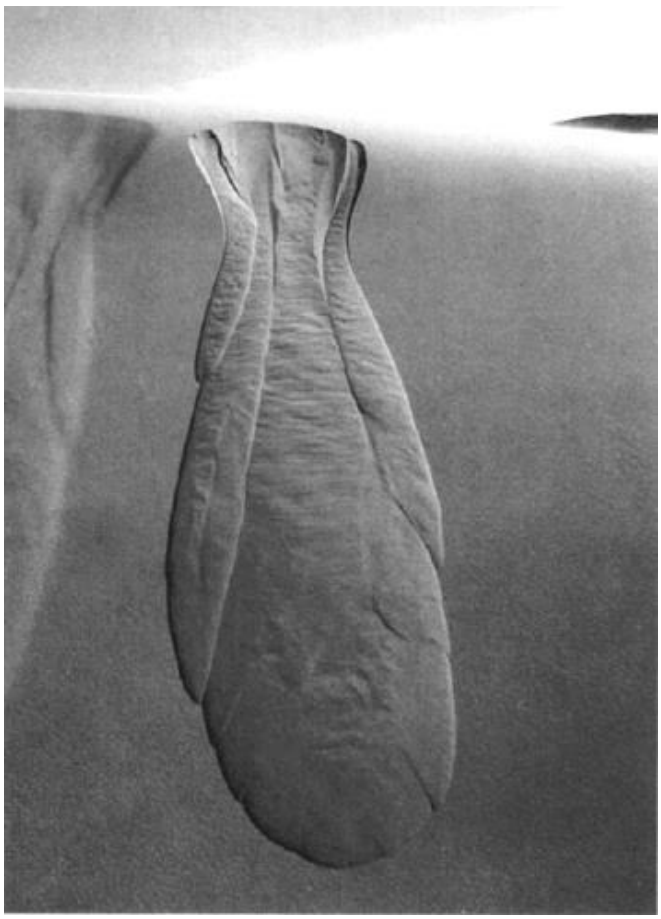

Figure 2.2 – A slow dry sand flow on the lee slope of a sand dune in the Namib Desert. (Hungr et al. 2001)

b) "*Sand (silt, debris, weak rock) flow slide* is a very rapid to extremely rapid flow of sorted or unsorted granular material on moderate slopes, involving excess pore pressure or liquefaction of material originating from the landslide source. Full or partial liquefaction of loose saturated granular material due to internal collapse during initial failure produces highly mobile, dangerous landslides. The term flow slide, introduced by Casagrande (1936), is suitable for this purpose. The detailed mechanism of motion of liquefied granular flow slides is often difficult to reconstruct from surface observations, as the liquefied zones are covered by drier or denser material. However, high velocity and long runout on relatively gentle slopes are clear distinguishing signs (Figure 2.3)."

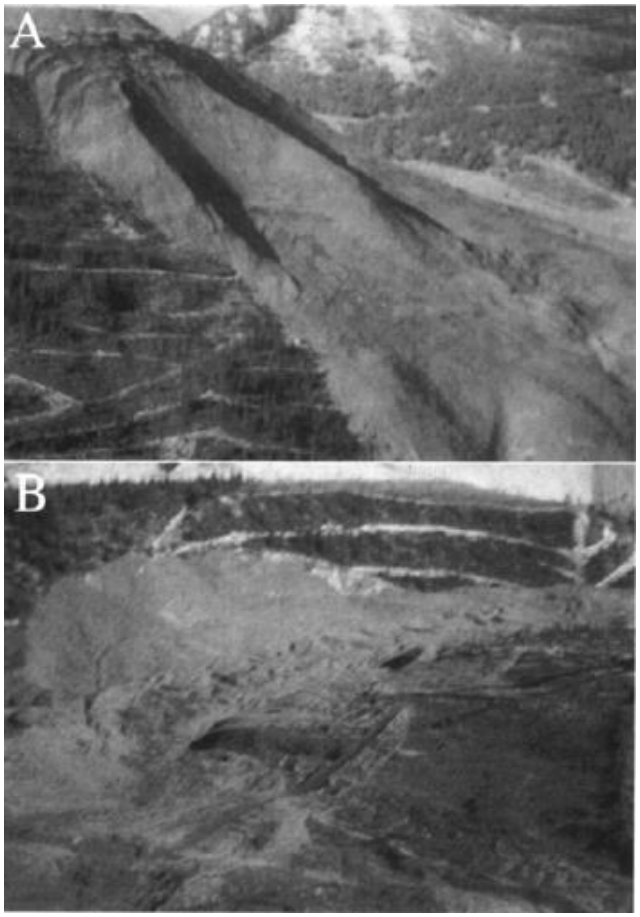

Figure 2.3 – A debris flow slide involving coal mine waste near Sparwood, British Columbia, Canada: (A) the source area with scarps and tension cracks surrounding the crown of the landslide; (B) a view from the slide crown down the flow slide path. (Hungr et al. 2001)

c) "*Clay flow slide* is a very rapid to extremely rapid flow of liquefied sensitive clay, at, or close to its original water content. Certain clays also exhibit structural collapse at failure, resulting in an extreme loss of strength and rapid motion. Clay flow slides initiate as retrogressive multiple rotational failures or as spontaneous sheet-like liquefaction failures (Figure 2.4 A). The flow may eventually become diluted upon entering a stream (Figure 2.4 B)."

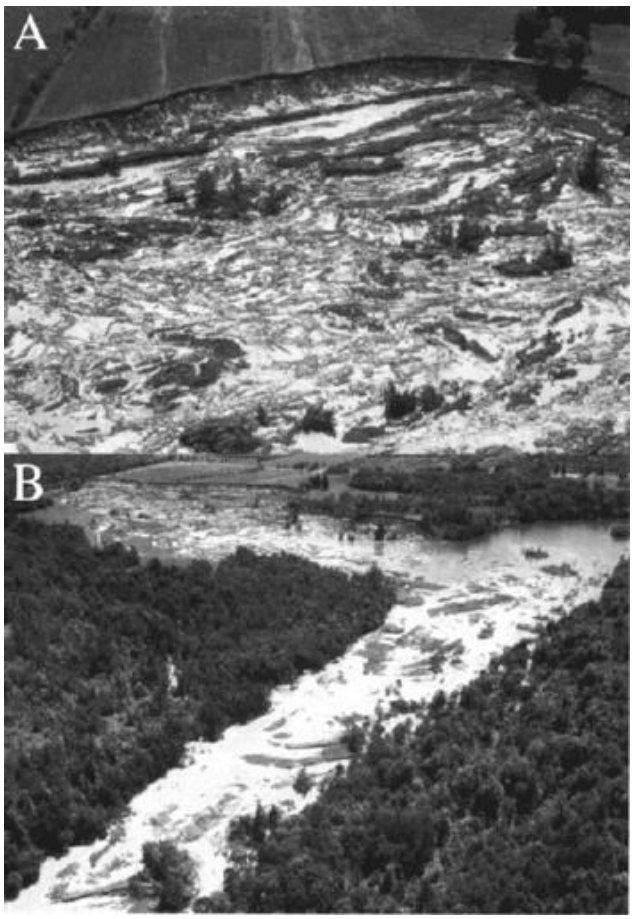

Figure 2.4 – A clay flow slide in extra sensitive marine clay at South Nation River, St. Lawrence Lowland near Ottawa, Canada: (A) source scar, with elongated slices of desiccated crust formed by retrogressive slumping; (B) clay flow slide in river channel, with the source scar in the background. (Hungr et al. 2001)

d) "*Peat flow* is a slow to very rapid flow-like movement of saturated peat, involving high pore pressures. A distinctive type of flow derives from the failure of peat deposits. It may be triggered by some external process causing rapid loading od a saturated peat layer or naturally by the breaching of an over-steepened rim of a raised bog. In either case, considerable pore pressure is inferred, to allow motion of a highly frictional organic material on gentle slopes."

e) "*Earth flow* is a rapid or slower, intermittent flow-like movement of plastic, clayey earth. If significant collapse-related pore pressure increase does not take place, clay landslides generally do not reach high velocities (Hutchinson 1970, Keefer and Johnson 1983). Nevertheless, disturbed, predominantly saturated clayey soil may accumulate on the slope in a tongue-like form (Bovis 1985). This type of flow characteristic of over-consolidated clays, weathered soft rocks and the weathering or erosion products derived from such deposits (Figure 2.5). Many earth flows tongues attain a certain steady-state condition, since material discharged downslope is periodically replenished through back-scarp retrogression in the form of slumps or falls."

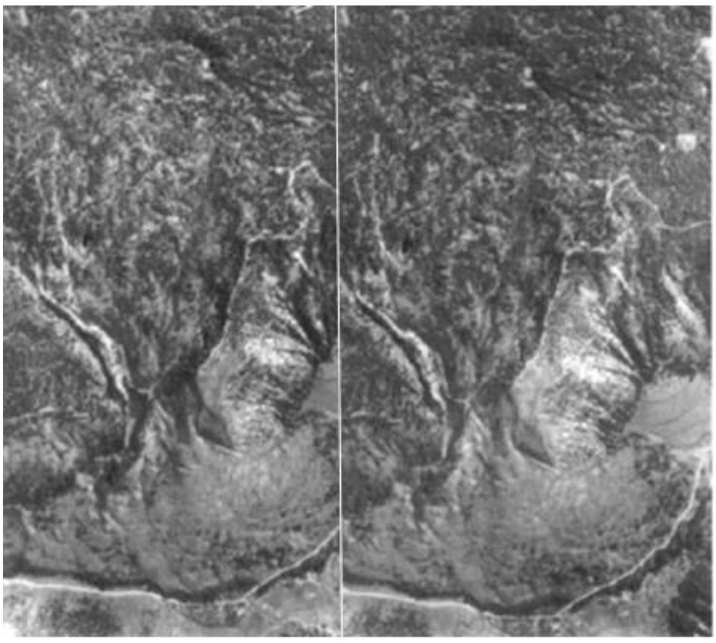

Figure 2.5 – A stereo view of a large earth flow at Pavilion, British Columbia. Note flow bifurcation into separate lobes, and prominent lateral deposits along the margins of each lobe. (Hungr et al. 2001)

f) "*Debris flow* is a very rapid to extremely rapid flow of saturated non-plastic debris in a steep channel. A debris flow event may occur in a series of surges, ranging in number from one to several hundred and separated by flood-like inter-surge slow (Pierson 1980). Using the rate of movement categories proposed by Cruden and Varnes (1996), the indicated movement rates for debris flows imply velocities in excess of 0.05 m/sec and up to 20 m/sec over much of their path (Figure 2.6). The key characteristic of a debris flow is the presence of an established channel or regular confined path. This is important because the channel carries surface water flow which is incorporated into the debris flow surges to increase their water content. Moreover, the lateral confinement helps to maintain fairly large flow depth and facilitates longitudinal sorting and surge development, and the existence of a regular path influences the approach towards practical hazard assessment for debris flow. A distinguishing characteristic of debris flows is the presence of a certain degree of rough sorting, which tends to bring the largest clasts close to the flow surface producing inverse grading (Costa 1984). The same process, combined with a strong vertical velocity gradient, also often leads to longitudinal sorting and the building of an accumulation of boulders and timber debris near the front of a surge (Pierson 1980, Iverson 1997, Figure 2.7). As a result of surging behaviour and the building of coarse surge fronts, peak discharges of debris flows are up to 40 times greater than those of extreme floods (Van Dine 1985, Hungr 2000). This gives debris flow considerable momentum and high destructive potential. Debris flows are fully saturated, with the possible exception of matrix-poor zones in the frontal boulder accumulations (Iverson 1997). Water content is a highly variable quantity due to the heterogeneity of debris flow surges and the transition from dense and coarse-grained surge front to more fluid inter-surge flow. Materials involved in debris flows range from clay to boulders several meters in diameter. In forested areas, as much as 80 percent of the volume may be organic material, such as timber (Swanston 1974)."

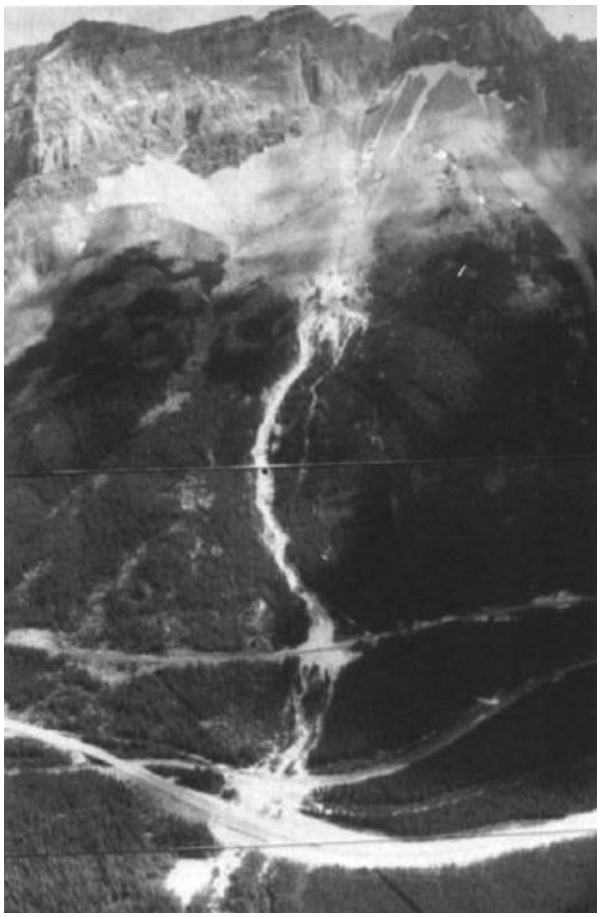

Figure 2.6 – The path of a 1984 debris flow at Cathedral Mountain, Yoho National Park, British Columbia, Canada, triggered by an outburst of water from a small glacier. (Hungr et al. 2001)

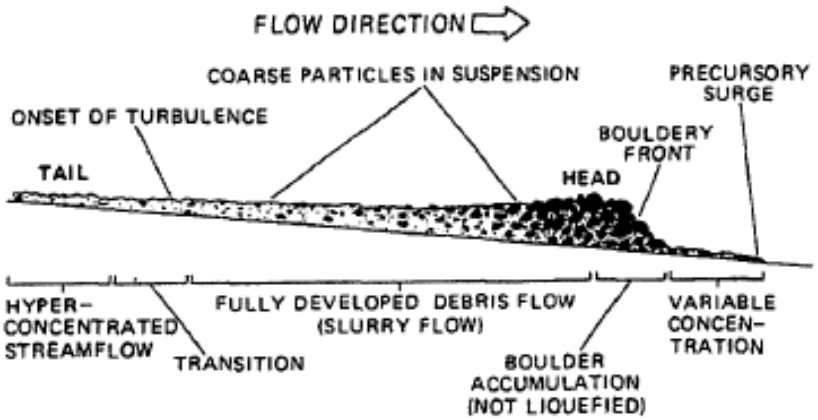

Figure 2.7 – The bouldery front of a debris flow surge (Pierson 1986)

g) "*Mud flow* is a very rapid to extremely rapid flow of saturated plastic debris in a channel, involving significantly greater water content relative to the source material. Under certain conditions, clayey colluvium can become diluted beyond its Liquid Limit. This may occur by sudden wetting of desiccated dispersive clays by rainstorms under arid conditions (Blackwelder 1928, Bull 1964). An important group of plastic mud flows occurs by gradual dilution of low plasticity clays derived from volcanic origins. The distinction between mud flows and debris flows is perhaps not of primary importance, as both have similar character. However, the clay fraction does modify the rheology of the material and this can be important in dynamic modelling (Takahashi 1991, Jordan 1994)."

h) "*Debris flood* is a very rapid, surging flow of water, heavily charged with debris in a steep channel. A debris flood may transport quantities of sediment comparable to a debris flow. The sediment may, furthermore, be transported in the form of massive surges, leaving sheets of poorly sorted debris ranging from sand to cobbles or small boulders. However, the sediment surges in a debris flood are propelled by the tractive forces of a water overlying the debris. As a result, the peak discharge of a debris flood is comparable to that of a water flood, perhaps multiplied by a bulking factor of between 1 and 2 (Costa 1984). The destructiveness of debris floods is similar to that of water floods. Objects impacted by debris floods are buried or surrounded by debris, but are often undamaged (Figure 2.8). An important exception to the above involves unusually high water-discharges, which exceed the discharge of major precipitation-related floods. Such discharges may result from a sudden breach of natural or man-made dams, glacier outbursts, catastrophic melting of snow cover on volcanos and similar events. In such cases, highly destructive discharges much in excess of major hydrological floods can occur, even in the rare case where no discharge magnification due to a build-up of a debris flow surge occurs (Figure 2.9, Skermer and Russel 1988). Debris floods can continue moving in channels with considerably flatter slopes than those required for debris flows and are, therefore, observed on larger streams. Strictly speaking, a debris flood is not a landslide, but a mass transport phenomenon."

Figure 2.8 – A truck engulfed by debris flood deposits in 1995 on the fan of Britannia Creek near Vancouver, Canada. The vehicle was largely undamaged. (Hungr et al. 2001)

Figure 2.9 – The effect of a catastrophic debris flood caused by an accidental damming of Britannia Creek, north of Vancouver in 1921, followed by a sudden release of 60,000 m3 of water, dammed behind a blocked railway culvert. (Hungr et al. 2001)

i) "*Debris avalanche* is a very rapid to extremely rapid shallow flow of partially or fully saturated debris on a steep slope, without confinement in an established channel. A debris avalanche begins as a more or less shallow surficial sliding failure on a slope and continues to develop into a rapidly moving wave-like flow, but does not move in an established channel. In its initial stages, before internal distortion and the development

of flow-like character, it may be referred to as a debris slide. Sharpe (1938) defined debris avalanche as a shallow landslide which is morphologically similar to a snow avalanche (Figure 2.10). Debris avalanches take place in various parts of a slope and do not normally occur repeatedly at the same location, since depletion of material usually occurs."

Figure 2.10 – A debris avalanche derived from shallow colluvium in an alpine area near Jasper, British Columbia, Canada. The debris avalanche started by a sliding failure of the colluvial veneer at the rime of spring snow avalanches which originated from the same slope.

j) "*Rock avalanche* is an extremely rapid, massive, flow-like motion of fragmented rock from a large rock slide or rock fall. Landslides deriving most of their volume from bedrock failure are often referred to as rock avalanches (Figure 2.11). The motion of rock avalanches is massive, in that the bulk of the rock fragments moves as a semi-coherent flowing mass. The term rock falls by contrast, should be reserved for talus-forming independent rolling, fall and bouncing of discrete rigid fragments, individually or in swarms. The source material of rock avalanche may be any kind of rock, sedimentary, metamorphic or igneous, including pyroclastic deposits. Weak rock masses appear to be more likely to produce slow moving rock slides than strong, brittle rocks."

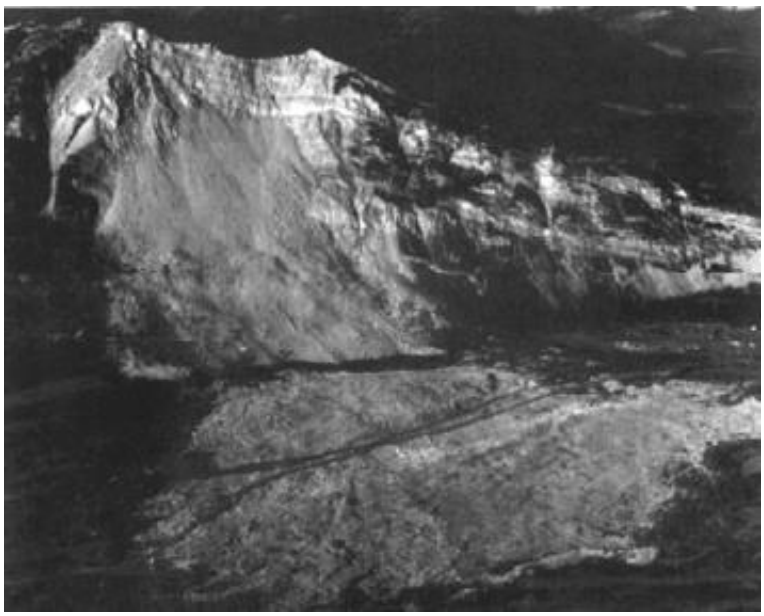

Figure 2.11 – The Frank rock avalanche of 1903, Alberta, Canada. The rock avalanche started by sliding along and across bedding joints and faults in Palaeozoic carbonate rocks (Hungr et al. 2001)

Landslides of the flow type present high variability of compositions and motion mechanism. In this work, it is analysed the behaviour of a channelised granular flow. For the time being, this experimental investigation was focused on dry sand, which is a sorted composition in the wide range of materials involved in flow-like landslides. Further studies would concern also the contributes of water content and the behaviour of plastic soils and unsorted debris mixtures. As mentioned before, according to Hungr et al. (2001), the channelised condition is a characteristic of debris flows, mud flows and debris floods. Those phenomena represent a real danger in many mountainous regions, offering natural streams and creeks. Albeit it is not a largely common composition for this kind of events, the use of dry sand is very convenient in experimental practice, as it guarantees repeatability and fast execution of tests. Moreover, it permits to investigate the fundamental behaviour of a fairly homogeneous and uniform granular flow from a physical point of view. Further analyses and simulations with continuum or discontinuum numerical models of this problem can be validated by the results obtained experimentally.

3. **Defensive structures**

To mitigate from impacts, structural defence measures are used to obstruct or retain landslides debris, reduce debris mobility or to deflect the direction of the flow. Defence measures may include single or multiple units of structures like rigid and flexible barriers, braking mounds, catching or deflecting dams and baffles (Kattel et al. 2018). Even if most of literature investigating deflecting dams is related to mitigation against snow avalanches, this type of structures is worth being further studied as a protection measure against any kind of granular material.

Category	Description
Td	**Direct impact zone of debris torrent:** Zone through which the high-energy debris front may travel; thus the risk of impact damage from one or more surges is high. Material transported through this zone could include boulders and rock fragments as much as several meters in diameter and logs tens of meters long
Ti	**Indirect impact zone of debris torrent:** Zone through which later surges may be potentially diverted and/or through which afterflow may travel; thus the risk of impact damage is lower. Material could include large rock and log debris, but is more likely to contain rock of less than 1 meter to fine-grained material and organic mulch
Tf	**Flood zone due to debris torrent:** Zone that is potentially exposed to flooding as a result of blockage of the main channel by debris torrent deposit. The risk of impact damage is low. Fine-grained material and mulch could be contained in the flood water

*From Thurber Consultants, Ltd. (1983).

Table 3.1 – Definition of hazard zones for debris flow hazard mapping. (Hungr et al. 1987)

As reported in Table 3.1, three hazard zones are distinguished: direct impact, indirect impact, and flood zone. The three zones correspond to the following hazard descriptions given by Hungr et al. (1987):

1. "Rapidly moving high-discharge surges in and immediately downstream of the transportation zone can destroy objects by violent dynamic thrust and impact."
2. "In the distal parts of the deposition zone, discharges and velocities are relatively low and impact loads are reasonably small; yet, large volumes of moving debris can bury areas and objects. Also, the liquid after-flow and flood discharges, being forced out of the normal channel by depositing surges, travel over and erode unprotected surfaces and deposit gravel and other fine debris."
3. "Downstream of the deposition zone, there is a relatively large area endangered by flooding when the inter-surge or post-event flood travels down some unexpected paths away from the regular channel."

A response to a natural hazard can be passive or active. Avoiding the risk area, without changing the event, represents a passive measure. Active measures instead are meant to mitigate the phenomenon and its impact. In Table 3.2 a classification of defensive measures against debris flow is reported (Hungr et al. 1987). Active protections are divided into three groups, based on the longitudinal position of application along the debris path.

Active measures in the source area, such as gullies and steep erodible reaches of creeks, involve reducing the unstable volume of material capable of flowing downstream. It reduces the number of potential points of initiation (Hungr et al. 1987). Usually, also other protections are installed in order to cooperate with the first ones. European practitioners use a series of check dams which stabilise the erodible segments, with a retention basin downstream (Eisbacher and Clauge 1984). In the transportation zone, active measures allow the channel to pass the debris surges downstream. Overflow and blockage may generate uncontrolled branching of subsequent surges. Confined channelisation can be used to elongate the transportation area downstream, and thus to protect area in correspondence of the original deposition area.

Measure	Purpose
Passive Measures	
Hazard mapping and zoning	Restrict use of endangered areas
Warning systems: advance, during event, or post-event	Facilitate evacuation at times of danger
Active Measures	
A. In source area	
Reforestation/controlled harvest	Reduce debris production due to logging or natural loss of forest cover
Forest road construction control	Eliminate unstable cuts and fills that could act as debris sources or initiation points
Stabilization of debris sources (channel linings or check dams)	Stabilize channel bed and side slopes in source reaches
B. In transporation zone*	
Training by chutes, channels, and deflecting walls or dikes	Ensure passage of debris surges down a predetermined path, without blockage or overflowing (branching)
Channel diversion	Change the path of debris flow away from endangered areas
Bridges designed for passage	Protect traffic on bridge and prevent channel blockage due to bridge obstruction
"Sacrificial" bridges or fords	Prevent channel blockage due to the obstruction of a bridge with inadequate clearance
Bypass tunnels beneath creek bed	Protect transportation route without modifying stream channel
C. In deposition zone*	
Open debris deposition basins; dikes or walls	Control the extent of a natural deposition area by shaping and diking
Closed retention barriers and basins: full or partial volume	Create a controlled deposition space fronted by a straining structure and a spillway
Bridges or other structures designed for burial	Prevent damage to structure during burial by debris flow
Debris sheds (galleries) or cut-and-cover tunnels	Place transportation route beneath deposition area

*The limits of transporation and deposition zones are understood as those applicable after the defensive measures are in place. Channels and chutes will move the point of deposition downstream, barriers and basins upstream.

Table 3.2 – Classification of defensive measures against debris flow. (Hungr et al. 1987)

As reported in Table 3.2, deflecting dams or dikes are very important to design, in order to avoid overtopping of the flume. Deflecting dikes are used in the deposition zone in order to laterally confine the deposits. Defence measures in the deposition zone are meant to control the areal size of deposition and to control the damage when deposition takes place. The purpose of closed debris basins is retaining a predetermined volume of debris while the associated water flow is drained through a discharge section (Hungr et al. 1987).

Another common protection measure is a retention system constituted by flexible barriers, as used against rockfall. A flexible barrier is commonly placed in the creek channel (Figure 3.1), and its ropes are anchored in the banks. Those structures allow large plastic deformations and hence energy dissipation, reducing the peak loads during impact (Volkwein et al. 2011). The permeability of the net implies that a fine part of debris flow is drained, while the rougher material is retained.

Figure 3.1 – Filled multi-level barriers in the Merdenson torrent, Switzerland. (Volkwein et al. 2011)

Debris flow creeks can also be diverted into better alignments in the transportation zone. On the side, this diversion could guarantee a reduction of magnitude for the future debris flow events (Hungr et al. 1987). Generally, several sources of debris are distributed along the flume, where the flow can initiate or increase. Diversions are meant to avoid those sources by channelling the water away.

Open basins permit to constrain a natural deposition of debris flow to predetermined later boundaries, upstream or downstream. Lateral dykes are installed nearly parallel with the flow direction and must be designed to contain the expected maximum depth of deposits, not only the flow depth. When the dikes are intended to deflect the flow away from the risk area, the flow runup height reached after the impact between the flow and the deflecting dam.

Figure 3.2 – A physical model test of marginal dams deflecting depositing debris from community of Port Alice on Vancouver Island. (Nasmith and Mercer 1979)

Figure 3.2 shows a physical model of a large-scale debris flow defence scheme in British Columbia, where a series of double lateral dams deflect depositing debris away from port Alice (Nasmith and Mercer 1979). The model tests suggested to double the dam, in order to prevent overtopping. In order to limit the downstream spread of debris deposition and to sharply deflect the debris flow away, terminal deflecting dams are constructed. For instance, Figure 3.3 shows a massive terminal dam used to protect a prison in the Fraser Valley (Martin et al. 1984).

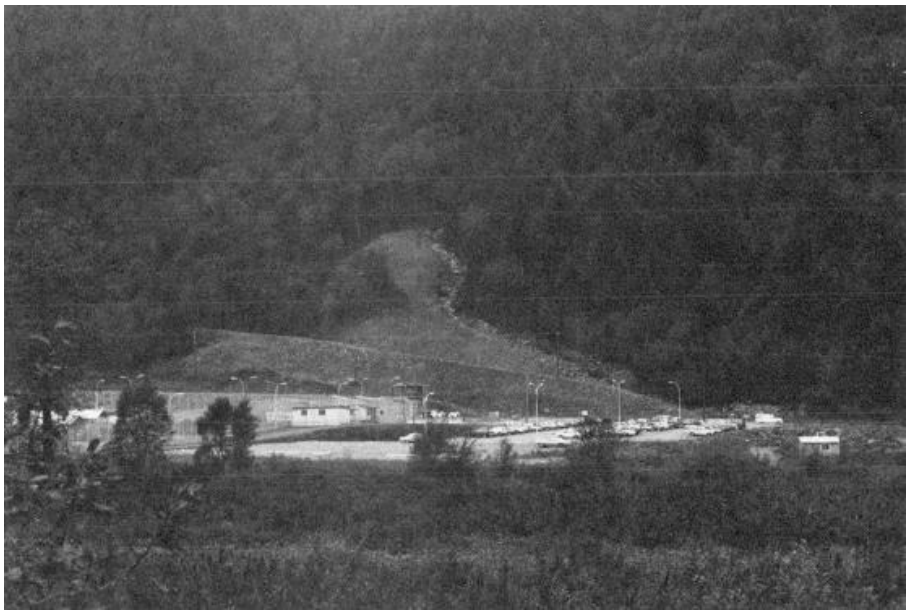

Figure 3.3 – Terminal deflecting dam protecting Agassiz correctional institution, Fraser Valley, British Columbia. (Hungr et al. 1987)

3.1 **The Froude number**

In order to design the height of a deflecting dam, the upstream Froude number Fr_1 represents an important dimensionless parameter, which is given by

$$(8) \quad Fr_1^2 = \frac{u_1^2}{h_1 \, g \cos \xi}$$

where u_1 is the speed and h_1 is the depth of the incoming flow, and ξ is the slope incline.

The Froude number Fr_1 measures the speed of the flow relative to the speed of the small amplitude surface waves. Flows are supercritical if $Fr > 1$, critical if $Fr = 1$, and subcritical if $Fr < 1$ (Gray and Cui 2007). In the experiments conducted by Hákonardóttir and Hogg (2005), and more generally for snow avalanches, the Froude number are $Fr \gg 1$. For example, Issler (2003) suggests that for dry-snow avalanches, Fr lies between 5 and 10. For debris flow, Hübl et al. (2009) point out that most field measurements of thrust forces have been carried out at relatively low velocities, with Froude numbers generally less than 2. According to GEO report 270 (Kwan 2012), only small-scale laboratory experiments, such as those carried out by Hübl and Holzinger (2003) have been made at higher Froude numbers.

4. Interaction between granular flow and deflecting dam

Gray et al. (1999c) state that steady oblique shocks can also develop in shallow granular avalanches by showing the measured avalanche velocity and thickness in a laboratory experiment on an inclined plane. These fields are determined form particle imaging velocimetry techniques and stereo-photogrammetric, respectively. Prior to the shock, the granular material flows downslope from left to right at approximately constant speed and with approximately constant thickness. An oblique shock is generated from the tip of the wedge. After the shock, the avalanche is about twice as thick as the incoming flow, the velocity magnitude decreases and the direction of the flow lies parallel to the wedge.

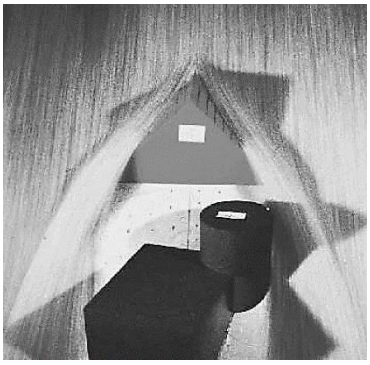

Figure 4.1 – Oblique shock and granular vacuum generated by a wedge (Gray et al. 1999c)

This is very similar to oblique shocks generated in shallow hydrodynamic flows. In the experiments the wedge is of finite length and an expansion wave forms immediately after it (Figure 4.1). The avalanche rapidly spreads in the fan and a granular vacuum forms in the lee of the wedge. Granular vacua often form in the lee of solid objects, and these grain free regions close only slowly in the wake as the pressure in the expansion waves is not strong.

Figure 4.2 – Oblique shock on an inclined plane chute (Gray et al. 2003)

Gray et al. (2003) show a steady-state oblique shock on a nearly non-accelerative slope inclined at $\xi = 33°$ to the horizontal. The shock is initiated by a sudden change in the sidewall angle, which points inward at an angle $\theta = 25°$ in the lower section of the chute. The oblique shock lies at an angle of approximately $\beta = 29°$ and the flow on the forward side of the shock is therefore confined to a very thin layer close to the deflecting sidewall. In the classical oblique shock problem, the field equations are satisfied by constant uniform state solutions, that are coupled together on either side of the shock by jump conditions (Gray et al. 2003). Experimental results of Hákonardóttir and Hogg (2005) are different from those of Gray et al. (2003), even though they are analysed using the same framework for modelling. Gray et al. (2003) reports a single experiment for which the upstream Froude number Fr_1 is 5.79. For such conditions, Hákonardóttir and Hogg (2005) evaluate the shock angle $\beta = 34°$, which differs from the calculation of Gray et al. (2003) because they did not explicitly use condition of continuity of tangential velocity across the shock u_2. Rather, they calculated the shock angle as a function of the downstream relative depth h_2 and the upstream Froude number Fr_1 (Hákonardóttir and Hogg 2005).

Figure 4.3 – Perspective view of an oblique shock (Cui et al. 2007)

Hákonardóttir and Hogg (2005) investigate the interaction between rapid, free-surface granular flows and deflecting dams by laboratory experimentation and by the formulation and analysis of a shallow-layer model of the motion. They consider the deflection of the uniform downslope flow by an impermeable, rigid barrier, orientated at an angle θ to the oncoming flow, finding that a steady solution may be derived where the flow undergoes an abrupt transition in flow states via an attached shock, which originates form the junction of the barrier and the lateral channel wall and which is orientated at an angle $\beta > \theta$. To analyse the transition, the authors assume that immediately downstream of the shock the motion is tangential to the barrier, and for their experiments the maximum distance between the shock and the barrier is sufficiently small so that the flow is unable to develop significantly and thus the assumption that is parallel to the barrier is reasonable.

Hákonardóttir and Hogg (2005), Gray and Cui (2007), and Cui et al. (2007) employ three jump conditions to determine the speed u_2 and the flow depth h_2 downstream of the shock, and the shock angle β, as functions of the upstream Froude number Fr_1 and the angle of deflection θ. The jump condition for conservation of mass implies that

$$h_1 u_1 \sin\beta = h_2 u_2 \sin(\beta - \theta) \quad (9)$$

while the tangential and normal conditions for the conservation of momentum yield

$$(10) \quad h_1 u_1^2 \sin\beta \cos\beta = h_2 u_2^2 \sin(\beta-\theta)\cos(\beta-\theta)$$

$$(11) \quad \frac{1}{2} h_1^2\, g \cos\xi + h_1 u_1^2 \sin^2\beta = \frac{1}{2} h_2^2\, g \cos\xi + h_2 u_2^2 \sin^2(\beta-\theta)$$

Eliminating u_2 from equations (9) and (10) gives

$$(12) \quad h_1 \tan\beta = h_2 \tan(\beta-\theta)$$

Substituting equations (9) and (12) into equation (11), eliminating h_2 and u_2, and using the definition (8) of Froude number we have a quadratic equation with respect to $\tan(\beta-\theta)$

$$(13) \quad Fr_1^2 \sin 2\beta \tan^2(\beta-\theta) - \tan(\beta-\theta) - \tan\beta = 0$$

which yields the shock-deflection angle relationship (Cui et al. 2007)

$$(14) \quad \theta = \beta - \tan^{-1}\left(\frac{1+\sqrt{1+8\,Fr_1^2 \sin^2\beta}}{2\,Fr_1^2 \sin 2\beta}\right)$$

for wedge angle θ as a function of the shock angle β and the incoming Froude number Fr_1.

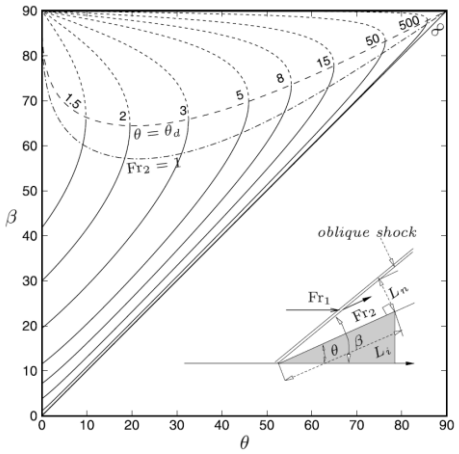

Figure 4.4 - Oblique shock-deflection angle curves: the solid curves denote weak shock solutions, and the short-dashed curves denote the strong shock solution (Cui et al. 2007)

According to Cui et al. (2007), for any given incoming $Fr_1 > 1$, there are two values of the shock angle β, provided the wedge angle θ is less than the detachment angle θ_d. The larger value of β corresponds to a strong shock, while the smaller value corresponds to a weak shock. Across the strong shock the downstream $Fr_2 < 1$ and the flow is subcritical, while across the weak shock $Fr_2 > 1$ and the flow is supercritical. This is important for both physical and numerical applications because it determines the appropriate number of boundary conditions. Since strong shocks are subcritical downstream, they always require both upstream and downstream boundary conditions. While most weak shocks are supercritical downstream and require only an upstream condition, which makes them naturally favoured to occur at deflecting dams. Cui et al. (2007) discussion therefore focusses on weak shocks, although it is possible to generate strong shocks by careful control of the upstream and downstream boundary conditions (Gray and Cui 2007). Weak and strong shock solution are separated by the detachment angle θ_d. For any Fr_1, if $\theta > \theta_d$, no solutions exist for a straight oblique shock, and the shock will be, instead, curved and detached.

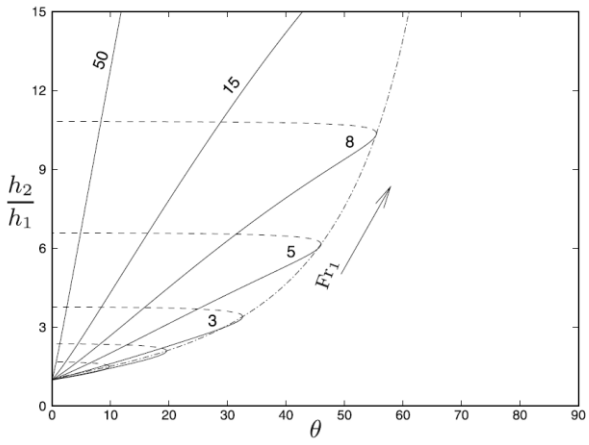

Figure 4.5 – Thickness ratio as a function of the wedge angle for a series of incoming Froude number values: the dash-dotted curve marks the transition θ_d (Cui et al. 2007)

The shock-deflection angle relationship (14) also solves for flow changes across shocks once β and θ are given.

Rewriting equation (12) yields an equation for the ratio of the thickness change across the shock

$$(15) \quad \frac{h_2}{h_1} = \frac{\tan\beta}{\tan(\beta - \theta)}$$

which shows that larger inflow Froude numbers Fr_1 and larger deflection angles θ lead to higher-thickness jumps for weak shocks.

Substituting equation (15) into equation (9) yields an equation for the ratio of the velocity magnitudes across the shock

$$(16) \quad \frac{u_2}{u_1} = \frac{\cos\beta}{\cos(\beta - \theta)}$$

which shows that, for weak shocks, the velocity ratio decreases with increasing deflection angle θ and upstream Froude number Fr_1.

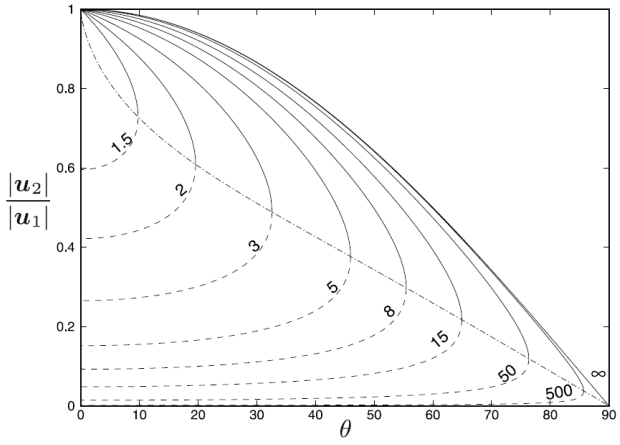

Figure 4.6 – Velocity magnitude ratio as a function of the wedge angle for a series of incoming Froude number values: the dash-dotted curve marks the transition θ_d (Cui et al. 2007)

The flow depth by the dam h_2 may be derived from

$$h_2 = \frac{\tan\beta}{\tan(\beta-\theta)} h_1 \quad (17)$$

$$\tan\theta = \frac{4\sin\beta\cos\beta\,(1 - Fr_1^2\sin^2\beta)}{-3 + 4\cos^2\beta\,(1 - Fr_1^2\sin^2\beta) - \sqrt{1 + 8\,Fr_1^2\sin^2\beta}} \quad (17)$$

as indicated by Hákonardóttir and Hogg (2005).

5. **Design criteria**

Irgens et al. (1998) presented a model based on the Voellmy-Perla equation to simulate snow avalanches impacting retaining dams at oblique angles of incidence, and then Harbitz and Domaas (1999) described the effects of natural deflecting dams on reported avalanches. A lumped mass model was used to calculate the path of the centre-of-mass along the side of a retaining dam. Strictly speaking, the centre-of-mass is representative of the frontal part of the slide, projected onto the terrain, since the total avalanche centre-of-mass may not even reach the dam. The equations are derived from classical mechanics, including a resistance force represented by a dynamic drag and a Coulomb friction. However, a lumped-mass consideration does not comprise any dynamic effects of the avalanche extension. Hence, the model results will anyhow be encumbered with obvious restrictions. For these reasons, it was preferable to perform a simplified-geometry study of the influence of avalanche-impact velocity, terrain inclination, dam configuration, and dam orientation on avalanche-course deflection and run-up height along a deflection dam (Figure 5.1).

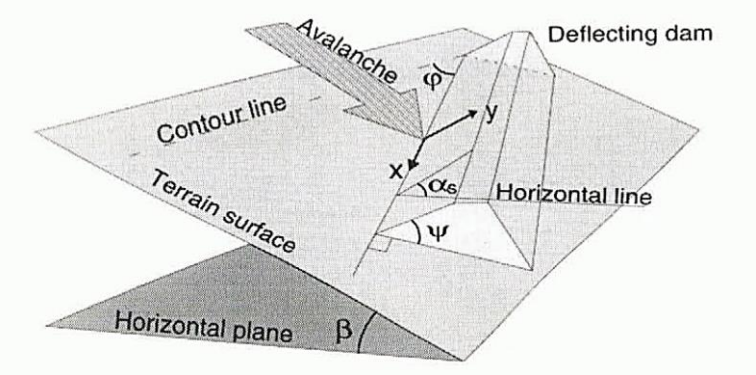

Figure 5.1 – Simplified geometrical configuration for the centre-of-mass model (Irgens et al. 1998)

The tangential and normal components of the centre-of-mass momentum equations are

$$(1) \quad \frac{du}{dt} = g_x \cos\gamma - g_y \sin\gamma - \mu g_z - \frac{D}{M} u^2$$

and

$$(2) \quad \frac{u^2}{R} = g_x \sin\gamma + g_y \cos\gamma$$

respectively, where u is the centre-of-mass velocity at time t, and g_x, g_y, g_z are components of the gravitational force per unit mass in the upper wall plane and its normal direction. γ is the angle between the centre-of-mass path tangent line and the base line, μ is the dry-friction coefficient, M/D is the mass-to-drag ratio, and R is the radius of curvature of the centre-of-mass path line on the wall. By means of the kinematic condition

$$(3) \quad \frac{u^2}{R} = -u \cdot \frac{d\gamma}{dt}$$

and the transcription

$$(4) \quad \frac{du}{dt} = \frac{du}{d\gamma} \cdot \frac{d\gamma}{dt}$$

equations (1) and (2) can be combined into

$$(5) \quad \frac{du}{d\gamma} = -u \cdot \frac{g_x \cos\gamma - g_y \sin\gamma - \mu g_z - \frac{D}{M} u^2}{g_x \sin\gamma + g_y \cos\gamma}$$

which is solved numerically.

The formulation of Irgens et al. (1998) is based on a centre-of-mass avalanche model and makes it possible to take into account the slope of the hill where the dam is located, the slope of the dam side, energy loss in the impact of the avalanche with the dam, and friction of the avalanche as it flows along the dam. Nevertheless, Jóhannesson (2001) states that this formulation is based on great simplifications of the flow of the avalanche during and after the impact with dam.

The traditional design of deflecting dams is based on centre-of-mass or rough energy considerations, which take no account of three-dimensional flow of the avalanche during the impact of the dam (Jóhannesson 2001). There is therefore a substantial uncertainty associated with the design of such dams.

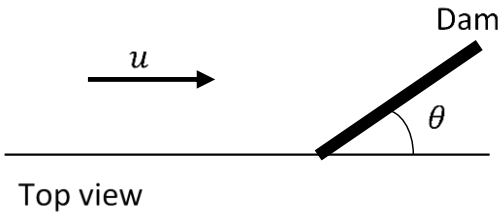

Figure 5.2 – Top view of incoming flow, at velocity u on a horizontal plane, impacting a deflecting dam with angle θ with respect to the flow direction. (Hákonardóttir and Hogg 2005)

Jóhannesson (2001) indicates that the dam height was chosen based on the traditional assumptions for the design of deflecting dams given by

$$(6) \quad h_u = \frac{(u \sin\theta)^2}{2g}$$

which expresses the run-up height of a point particle, travelling at speed u on a horizontal plane, which hits a deflecting dam under a deflecting angle θ (Figure 5.2). It is assumed that no energy is lost during the impact of the particle with the dam, nor due to friction with the dam as the particle moves along the dam after the impact.

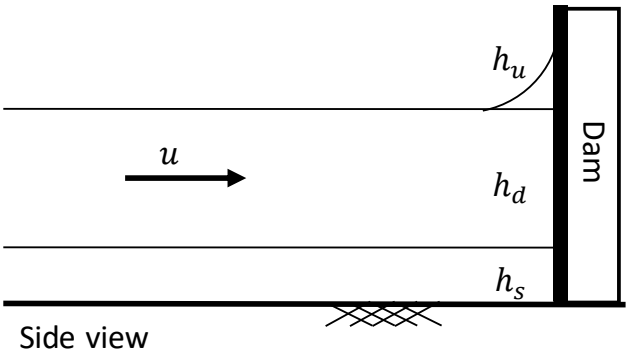

Figure 5.3 – Side view of incoming flow depth, as a sum of three thicknesses, impacting a deflecting dam at velocity u.

The design height h_D is then determined from the equation

$$(7) \quad h_D = h_s + h_d + h_u$$

where h_s and h_d are estimates of the thickness of snow on the ground and the thickness of the dense part of the flowing avalanche, respectively (Jóhannesson 2001, Jóhannesson et al. 2009, Figure 5.3).

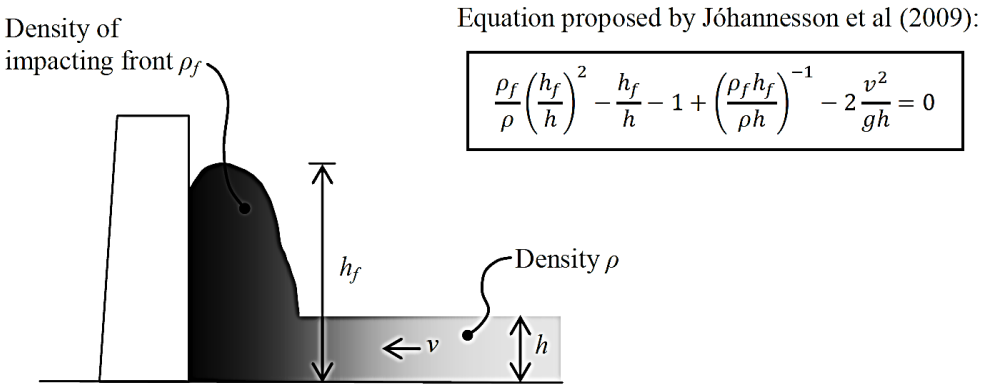

Figure 5.4 – Calculation of debris runup height h_f based on the momentum equation (Kwan 2012)

Kwan (2012) indicate that debris runup height, against vertical rigid barrier, can be calculated using energy principle (6), which gives a conservative estimate, as it assumes no energy loss during the runup process. However, Jóhannesson et al. (2009) have developed an analytical solution for the calculation of debris runup height against vertical barrier on a horizontal channel bed (Figure 5.4), which expresses the relationship between h_f/h and Froude number given by the analytical solution (Kwan 2012). The equation is derived from conservation of mass and momentum for a shock that occurs during the impact of a shallow flow layer on vertical rigid barrier, and is considered suitable for debris runup height calculation.

Choi et al. (2015) reported several experimental data, which are compared with the two theoretical functions in use for design purpose. Measured data points confirm the theoretical predictions and show that for sand flow the energy principle is suitable, while for water flow the momentum equation is more appropriate (Figure 5.5).

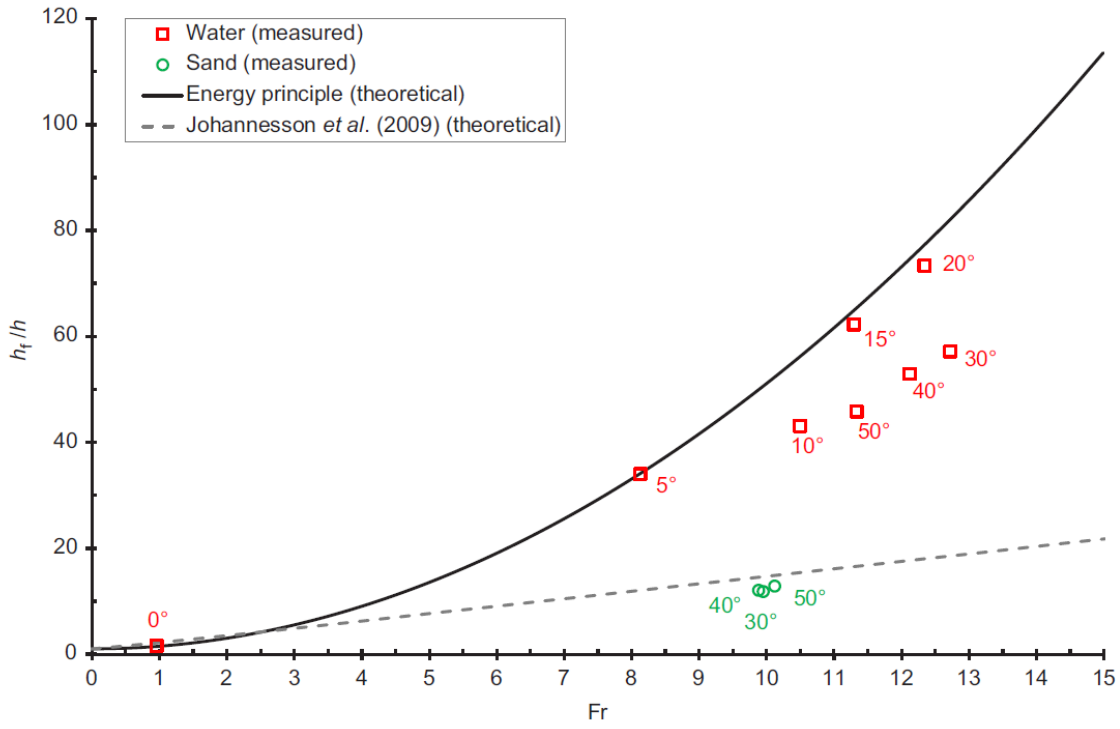

Figure 5.5 – Experimental data points compared with main design guidelines for runup height (Choi et al. 2015)

It is noted that this equation gives a runup greater than (6) when Fr < 2.5, and in such circumstance, the debris runup height given by the energy principle may be more appropriate for design purpose. When Fr > 2.5, runup height can be assessed using the analytical solution (Kwan 2012). The assessment of runup height for flow on an inclined bed using equation by Jóhannesson et al. (2009) may not be applicable, in which case the use of energy principle should be considered (Figure 5.6).

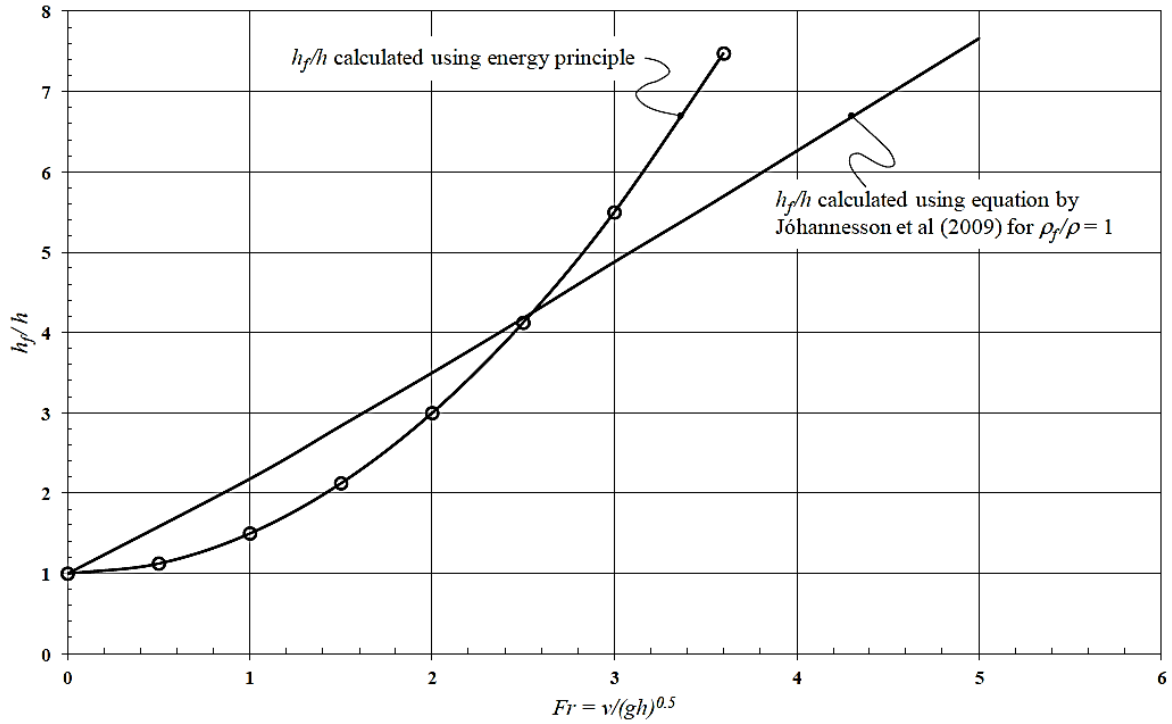

Figure 5.6 – Relationship between normalised runup height and Froude number of debris flow calculated using equation by Jóhannesson et al. and energy principle in case of horizontal bed and vertical barrier (Kwan 2012)

6. **Physical modelling**

The work is intended to understand how a system of two deflecting dams would work, how effective they would be at retaining the flow and at dissipating its energy, and what is the role played by geometry.

This modelling aims to a better comprehension of the interaction between dry granular flows and oblique obstacles. The flow behaviour is studied along a small-scale flume, which presents two deflecting dams downstream. The flow depth and velocity distribution along the flume are measured, as well as the run-up height, under different geometrical configurations of the deflecting system.

6.1 **Small-scale flume**

The physical model consists in a 4.5 m long flume, which is 200 mm wide and 500 mm deep (Figure 6.1). Assuming that the slope of the avalanche path near the obstacle is about 10°, which, in most cases, is the start of the runout area or protection zone (Primus et al. 2004), considering the dams perpendicular to the base of the flume is a good approximation of a site configuration.

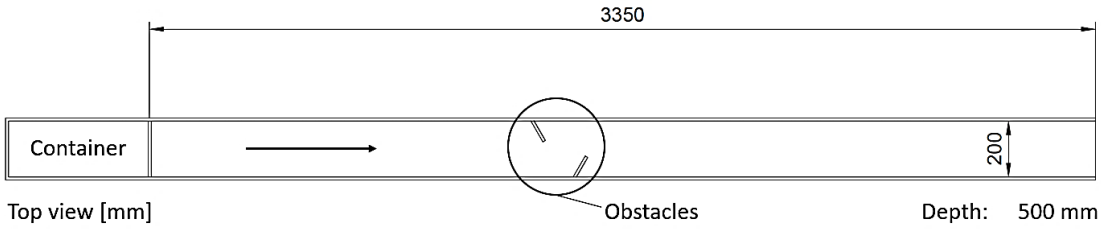

Figure 6.1 – Physical model scheme

The acrylic base and side walls are supported by an aluminium frame. The channel is composed by an upstream segment constituting the 1.15 m long container, where material is poured and stored, and by a downstream segment constituting the 3.35 m long chute, where the material

slides. The gate dividing the two segments is locked at the bottom by a magnet, and its opening is controlled by an air pressure circuit. The first dam is placed at 1.25 m from the gate. A receiving container is placed downstream to collect the material flowed down.

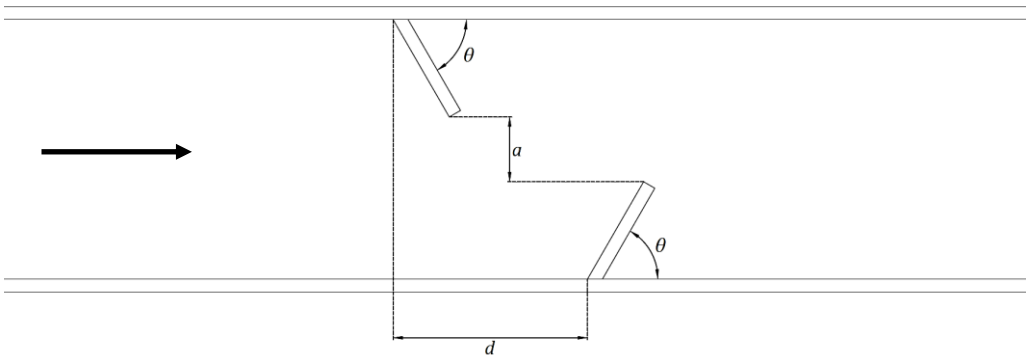

Figure 6.2 – Top view geometry of the deflecting system defined by aperture a, deflection angle θ and spacing d

The geometry of the system is totally defined by three main parameters: the aperture a, the deflection angle θ, and the spacing d (Figure 6.2).

Figure 6.3 – Small-scale flume physical model (Hong Kong UST)

Top cameras were used to observe the motion and measure the velocity of the centreline of the flow, which is less subjected to the side walls disturbance, and lateral cameras measured the depth of the flow and the run-up by the dams. The flow motion is recorded thanks to five GoPro cameras, two (240 frame per second) placed on top of the chute orthogonal to the base, two (240 fps and 120 fps) on the side orthogonal to the lateral wall, and one (120 fps) downstream orientated toward the front of the flow.

The instrumentation setup is intended to measure the flow velocity in four different points, the maximum and the residual flow depths by the dam, and to check potential differences between the two runups. The retained mass is separated from the rest of material, which slid downstream, and then individually weighted by a balance (0.1 kg of accuracy).

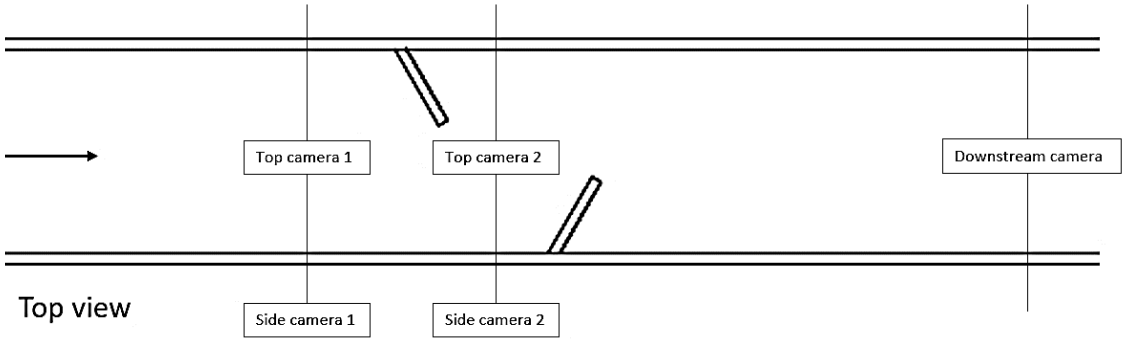

Figure 6.4 – Setup scheme of recording

The acquisition of kinematic data was conducted with the open source software Tracker 5.1.2 by video analysis. The videos were calibrated thanks to square grid drawn on the base (50 mm) and the square grid drawn on the side wall (30 mm) of the flume.

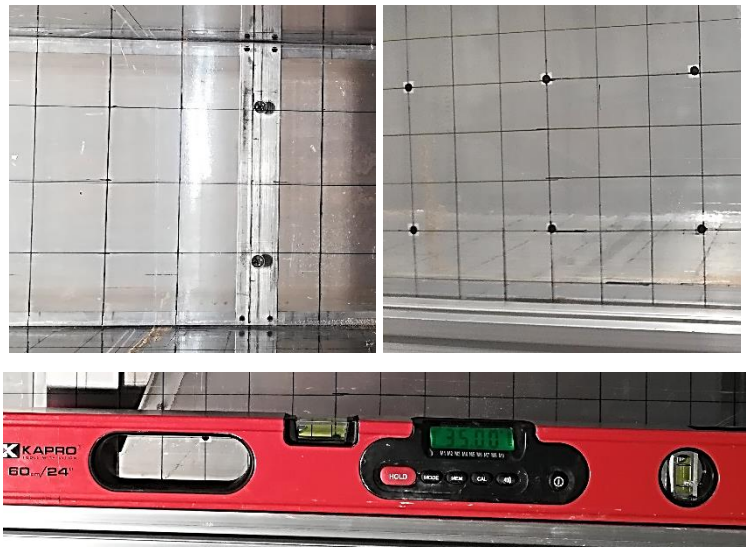

Figure 6.5 – Details of the 50-mm basal square grid (left) and the 30-mm lateral square grid (right) and the level with digital display (bottom)

The free flow control test and the main series test were conducted with the same initial configuration, pouring m_{tot} = 45 kg of dry sand in the upstream container and then lifting up the chute incline to ξ = 35° with respect to the horizontal. The right slope incline was checked by a level with digital screen (0.05° of accuracy) placed on the channel before every test. The material used for the tests was dry Toyoura sand, whose properties are reported in Table 6.1 below.

Mean grain size d_{50} [mm]	0.16
Coefficient of uniformity C_u	1.46
Solid density ρ_s [g/cm^3]	2.64
Critical friction angle φ_c [°]	31
Basal friction angle φ_b [°]	21

Table 6.1 – Toyoura sand properties (Herle and Gudehus 1999)

In total, seventeen tests were run, as reported on the test plan in Table 6.2, constituting a physical parametric study.

Test Series	Test ID	Aperture a [mm]	Angle θ [°]	Spacing d [mm]	Objective / Description	
Control	free-flow	-	-	-	Remark: undisturbed flow	
1	a25-θ90-d000	25	90	0	Influence of different spacings	Influence of different angles
2	a25-θ90-d150			150		
3	a25-θ90-d300			300		
4	a25-θ75-d000		75	0	Influence of different spacings	
5	a25-θ75-d150			150		
6	a25-θ75-d300			300		
7	a25-θ60-d000		60	0	Influence of different spacings	
8	a25-θ60-d150			150		
9	a25-θ60-d300			300		
10	a00-θ90-d000	0	90	0	Remark: full cross section	
11	a00-θ90-d150	0	90	150	Influence of different spacings	Influence of different angles
12	a00-θ90-d300			300		
13	a00-θ75-d150		75	150	Influence of different spacings	
14	a00-θ75-d300			300		
15	a00-θ60-d150		60	150	Influence of different spacings	
16	a00-θ60-d300			300		

Table 6.2 – Detailed test plan

6.2 **Results**

Figure 6.6 shows a typical flow depth evolution around the barrier when d = 0. At the impact, the undisturbed flow increases its depth by the dam (top left), while a wake flows down through the aperture between the obstacles. Then, a wave propagates upstream (top right and centre left) increasing the flow depth toward an almost linear distribution (centre right), while the flow depth reaches its maximum value by the dam. Finally, the flow starts losing thickness (bottom left) and the sand flows down completely, with the exception of the residuals by the dams (bottom right).

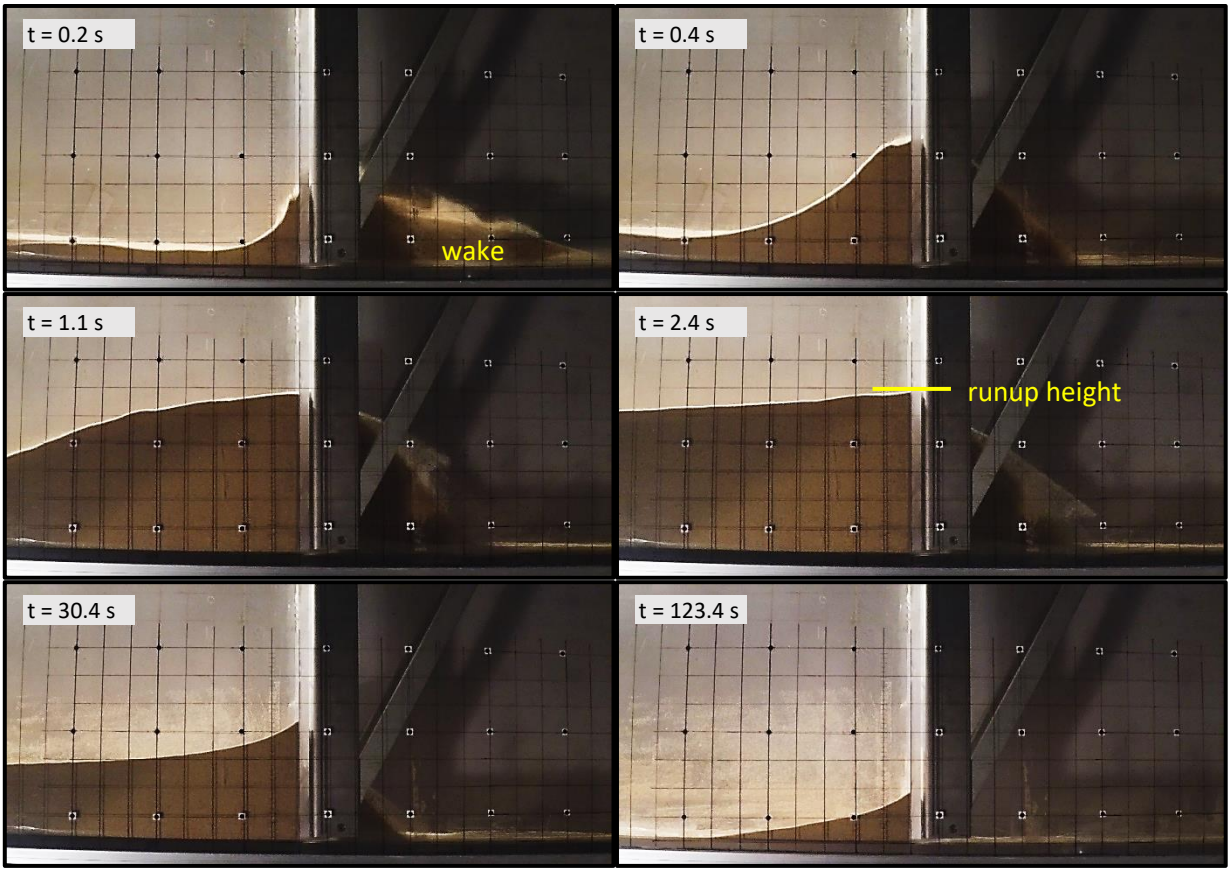

Figure 6.6 – Example of progressive side view of flow depth distribution in case of d = 0 (test a25-θ60-d000). The frame just before the impact represents t = 0.

In Figure 6.7 it is illustrated a side view progressive distribution of flow depth in case of dams at different longitudinal position ($d \neq 0$). At first the flow impacts the two barriers generating an increment of height (centre left and right), then the depth by the dam reaches its peak while a wave propagates upstream (top right). This mechanism increases the upstream flow depth from the initial value of about 40 mm to a peak of 150 mm, marking a substantial change ratio of 3.75 times. However, it never reaches the peak depth by the dam of 180 mm that corresponds to a change ratio of 4.50 times. After propagating enough upstream (bottom left) the flow depth decreases until the final equilibrium is reached (bottom right).

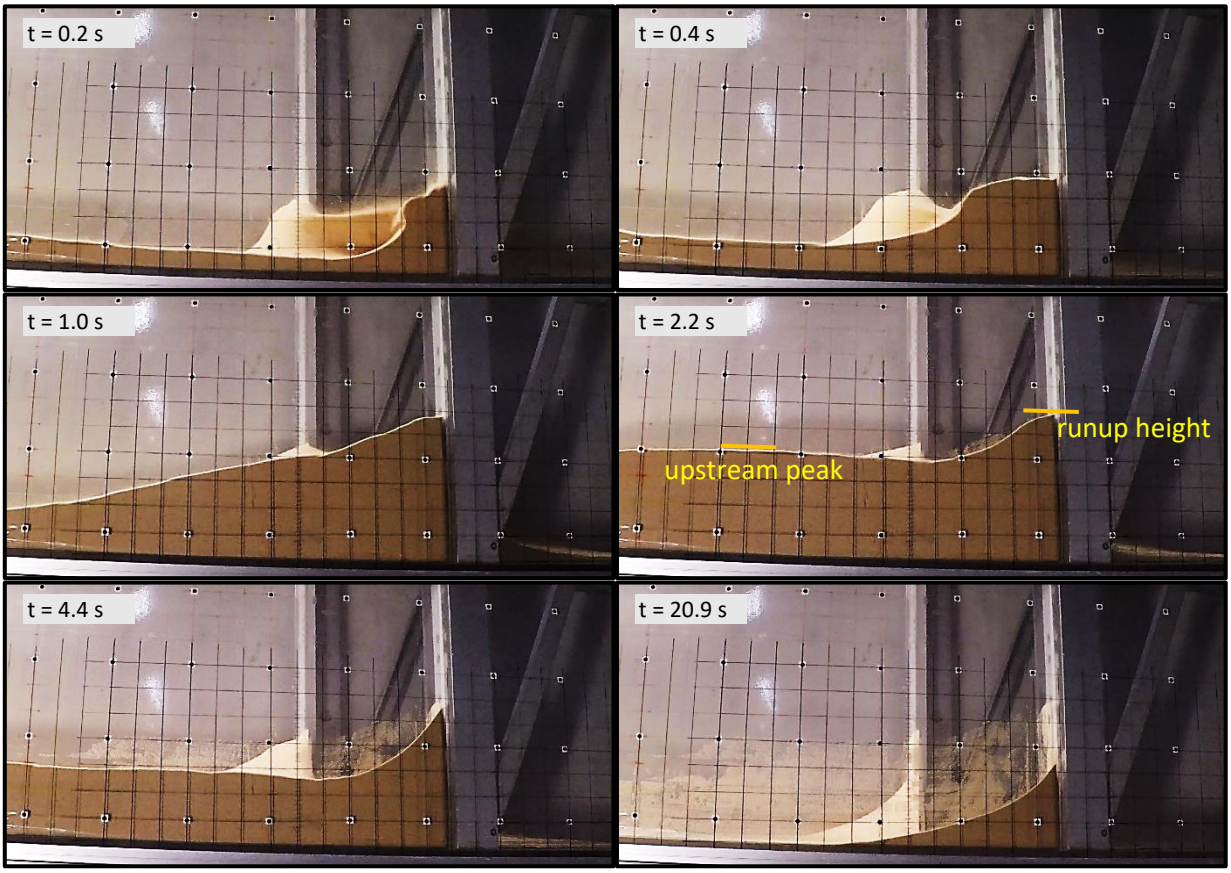

Figure 6.7 – Example of progressive side view of flow depth distribution in case of $d \neq 0$ (test a25-θ90-d150). The frame just before the impact represents t = 0.

Figure 6.8 illustrates the flow differences in top view between the case of dams at the same longitudinal position ($d = 0$) and the cases of dams with spacing ($d \neq 0$). Clearly, the first case is characterised by a longer time necessary to let the sand flow down, because the space between the obstacles is smaller than the others.

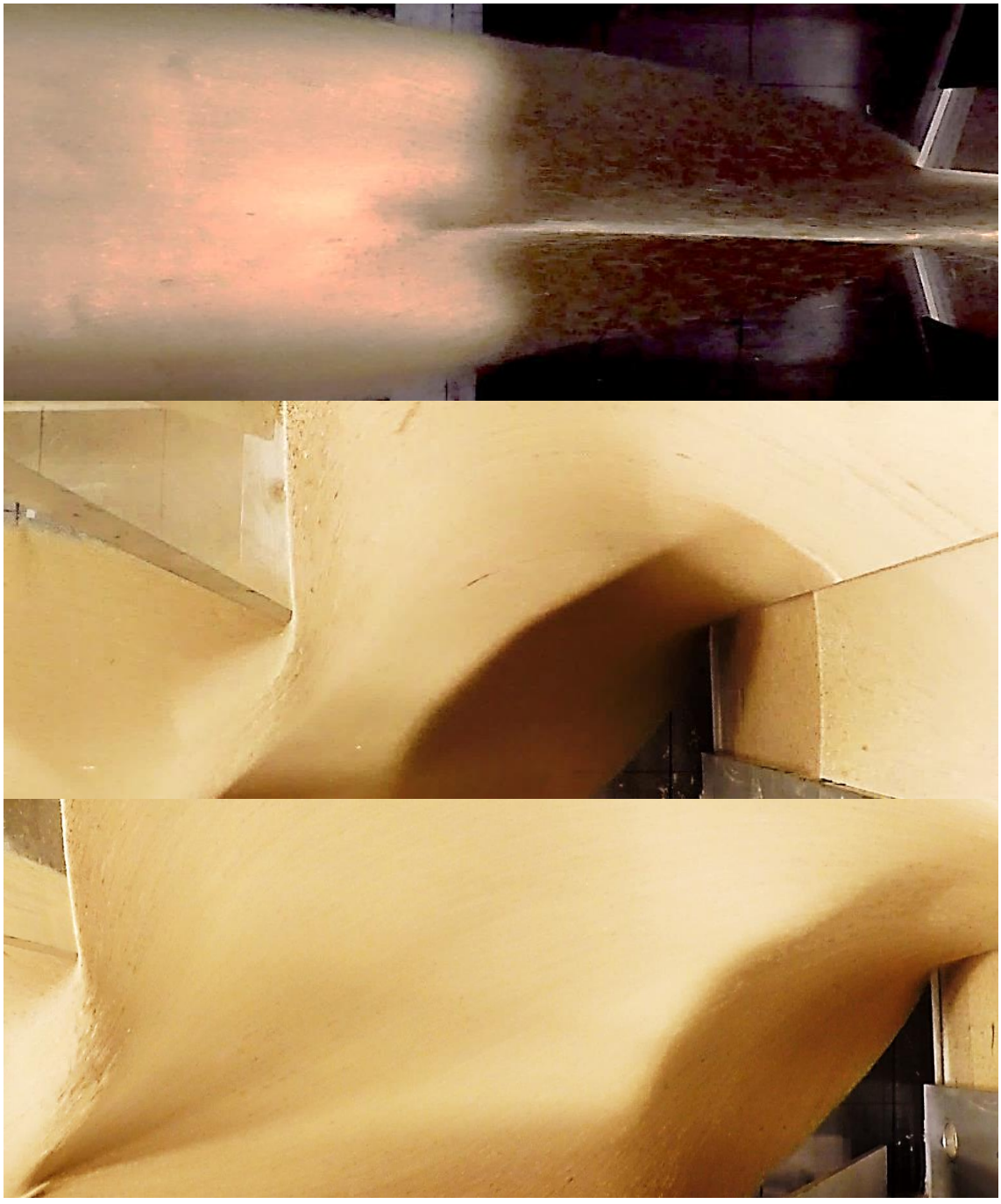

Figure 6.8 – Differences in top view between the cases of $d = 0$ (top), $d = 150$ (centre), and $d = 300$ (bottom)

In Table 6.3 are reported all the maximum depths and peak change ratio registered by the dam, which are approximately equal on both the side of the system, as the downstream camera confirms. It is remarkable how close they are to the value obtained for the traditional full section barrier (a00-θ90-d000). That may be due to the discontinuous nature of sand, that is probably not that much influenced in the mechanism of runup by the material on its side.

Test ID	Depth	
	h_r [mm]	h_r/h_0
a25-θ90-d000	175	4.38
a25-θ90-d150	170	4.25
a25-θ90-d300	165	4.13
a25-θ75-d000	175	4.38
a25-θ75-d150	165	4.13
a25-θ75-d300	160	4.00
a25-θ60-d000	170	4.25
a25-θ60-d150	160	4.00
a25-θ60-d300	160	4.00
a00-θ90-d000	180	4.50
a00-θ90-d150	180	4.50
a00-θ90-d300	180	4.50
a00-θ75-d150	180	4.50
a00-θ75-d300	165	4.13
a00-θ60-d150	175	4.38
a00-θ60-d300	160	4.00

Table 6.3 – Maximum flow depths by the dam

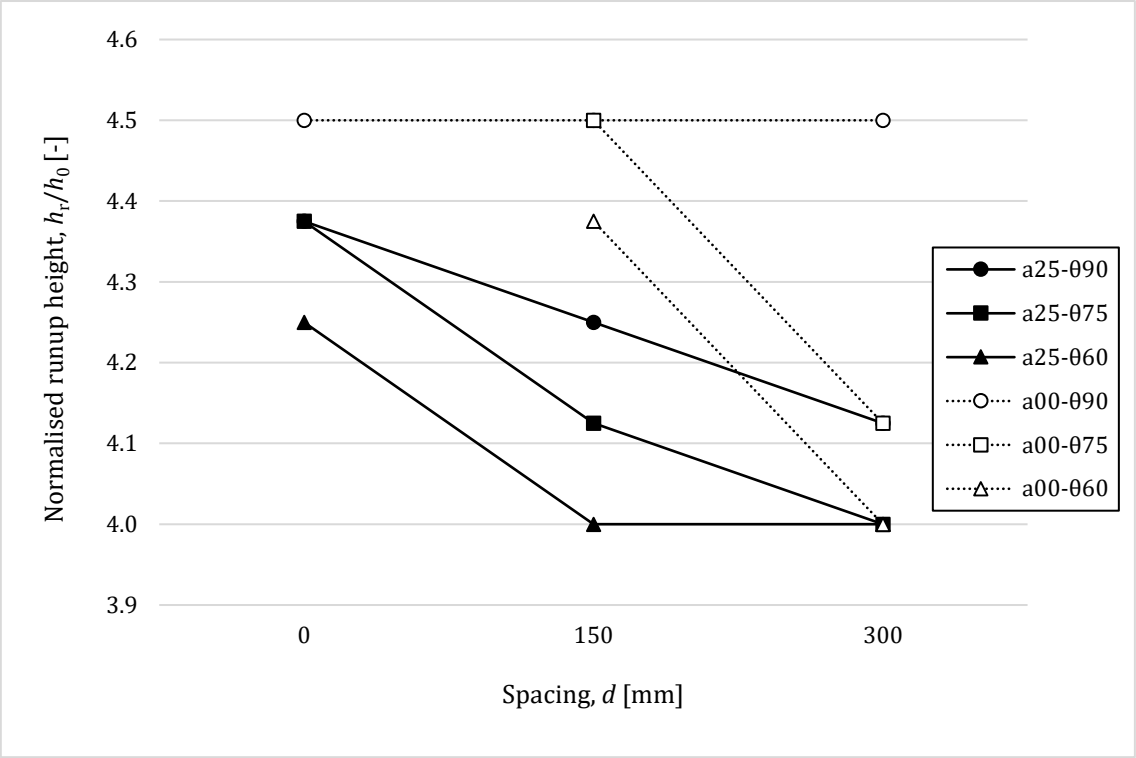

Figure 6.9 – Maximum depth h_r by the dam for different spacings d

In Figure 6.9 it is shown how the runup on the dam changes as a function of the spacing. With special reference to the cases of a = 25 mm the relationship between h_r and d in clearly inverse. It is also evident the slight role played by the deflection angle θ, whose increment is associated with an increment of the runup. With a = 0 mm also, the same dependencies can be suggested by the diagram, but those results are less clear. It is remarkable how with a = 0 mm and θ = 90° the runup is not affected at all by the spacing, differently from the other cases.

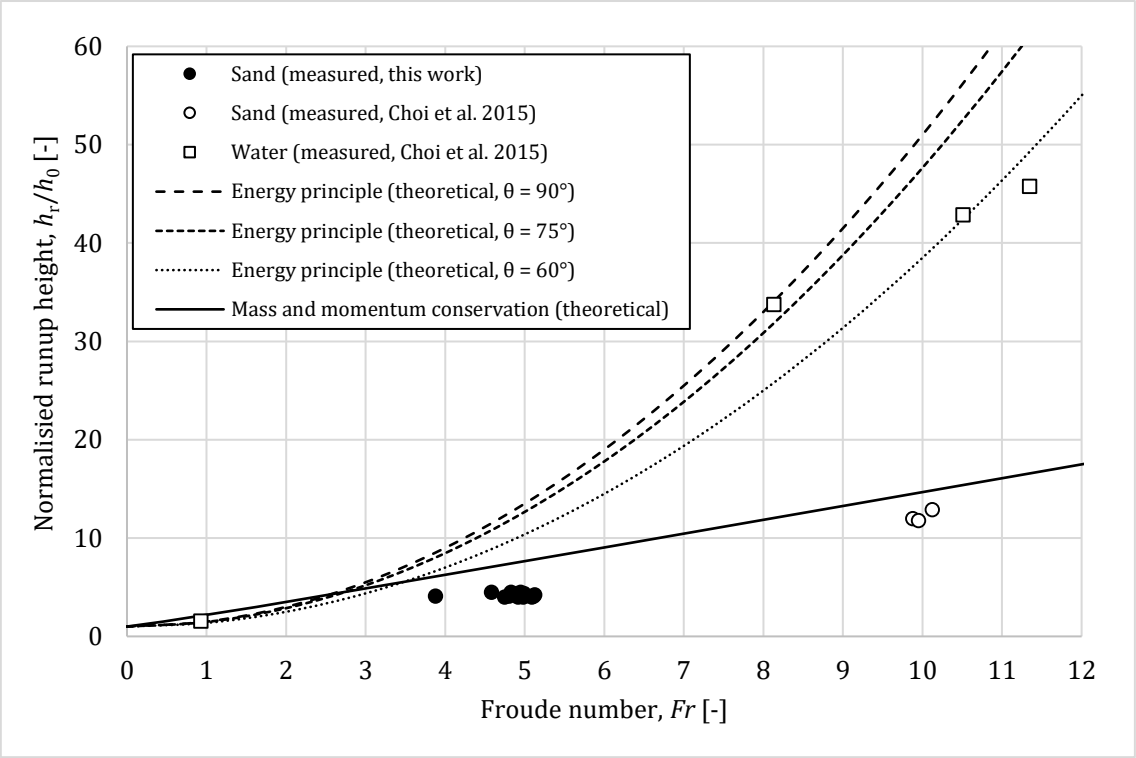

Figure 6.10 – Runup height design criteria for horizontal bed compared with experimental results

In Figure 6.10 the normalised runup height is compared with the traditional design criteria based on conservation of energy for a particle mass travelling on a horizontal bed. It is also reported, in the hypothesis of unchanged density, the theoretical solution proposed by Jóhannesson et al. (2009) which is based on mass and momentum conservation across the shock observed by the dam. As Choi et al. (2015) verified for *Fr* = 10, the energy principle is overconservative even for *Fr* = 5. As a matter of fact, according to Kwan (2012), it should be preferred the solution of Jóhannesson et al. when Fr > 2.5. It is remarkable that all the points collected in this work suit well that design criterion, even though they are referred to different deflecting angles.

Regarding the retaining capacity of the deflecting system, in Table 6.4 are shown the retained mass m_{ret} and the residual depth h_{res} by the dam. The balance was not able to give a more precise value for the retained mass, but the order of magnitude is clearly around 1 kg (mean 0.93 kg,

maximum deviation 0.37 kg) for all the different tests, which suggests that the retaining capacity is not that much affected by the geometric configuration of the system.

It is remarkable that the highest percentages of retained mass m_{ret}/m_{tot} are registered for $a = 0$, which is sensible since in this case the barrier has more space to store the grains. As a matter of fact, those m_{ret} peak values correspond to the residual depth h_{res} peaks.

Test ID	Retaining capacity			
	m_{ret} [kg]	m_{ret}/m_{tot} [%]	h_{res} [mm]	h_{res}/h_0 [-]
a25-θ90-d000	1.0	2.22	95	2.375
a25-θ90-d150	0.8	1.78	90	2.250
a25-θ90-d300	0.9	2.00	80	2.000
a25-θ75-d000	0.9	2.00	65	1.625
a25-θ75-d150	0.8	1.78	60	1.500
a25-θ75-d300	0.7	1.56	60	1.500
a25-θ60-d000	0.9	2.00	55	1.375
a25-θ60-d150	0.8	1.78	55	1.375
a25-θ60-d300	0.8	1.78	50	1.250
a00-θ90-d150	1.2	2.67	100	2.500
a00-θ90-d300	1.3	2.89	105	2.625
a00-θ75-d150	1.0	2.22	70	1.750
a00-θ75-d300	0.9	2.00	70	1.750
a00-θ60-d150	0.9	2.00	60	1.500
a00-θ60-d300	1.0	2.22	60	1.500

Table 6.4 – Retaining capacity details

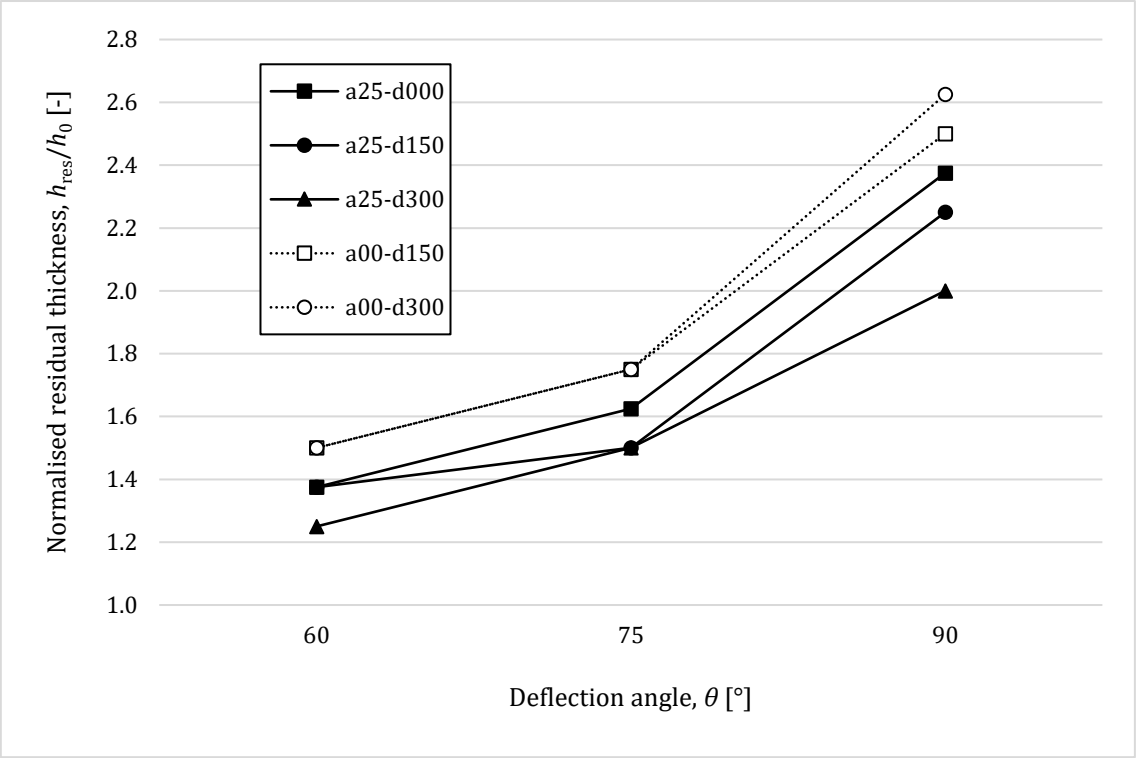

Figure 6.11 – Residual thickness h_{res} dependency on deflection angle θ

From Figure 6.11 it is evident that the residual thickness h_{res} depends on the deflection angle θ with an increasing relationship. The diagram also confirmed that the cases with aperture $a = 0$ present a better capacity of retaining material, since their residual thickness is higher than the other cases in every point.

With exception of test a25-θ90-d300, the initial velocities of all the tests are in good agreement with the one measured in the free flow control test. To validate the magnitude of those velocities, a hand calculation based on conservation of mechanical energy was carried out. Assuming no mass change and no energy loss due to friction, the theoretical velocity would be around 3.5 m/s, which is not that much higher than the ones measured. Without considering test a25-θ90-d300, the average velocity is about 2.8 m/s and the respective incoming Froude number is almost 5, which implies a supercritical condition.

Test ID	Incoming front velocity u_1 [m/s]	Incoming Froude number Fr_1
free-flow	2.965	5.23
a25-θ90-d000	2.782	4.91
a25-θ90-d150	2.905	5.12
a25-θ90-d300	2.198	3.88
a25-θ75-d000	2.741	4.83
a25-θ75-d150	2.723	4.80
a25-θ75-d300	2.786	4.91
a25-θ60-d000	2.763	4.87
a25-θ60-d150	2.822	4.98
a25-θ60-d300	2.884	5.09
a00-θ90-d000	2.807	4.95
a00-θ90-d150	2.598	4.58
a00-θ90-d300	2.804	4.95
a00-θ75-d150	2.736	4.83
a00-θ75-d300	2.898	5.11
a00-θ60-d150	2.830	4.99
a00-θ60-d300	2.691	4.75
Average	2.796	4.93

Table 6.5 – Initial front velocities, respective Froude numbers, and their average values, calculated not considering test a25-θ00-d300

Since every test is subjected to a slight natural variability, all the results are presented normalised by the initial velocity of the respective test in order to allow a dimensionless comparison. The normalised velocities are

$$U_1 = 1\,, \quad U_2 = \frac{u_2}{u_1}\,, \quad U_3 = \frac{u_3}{u_1}\,, \quad U_4 = \frac{u_4}{u_1}$$

Considering the first dam as the zero point of the longitudinal axis, in Table 3.6 are reported the surveyed velocities, normalised by the initial velocity u_1 registered at x_1 = –100 mm before the first dam. The second velocity u_2 is measured around x_2 = 50 mm, the third velocity u_3 around x_3 = 200 mm, and the fourth velocity u_4 around x_4 = 350 mm.

Test ID	Normalised front velocity		
	u_2/u_1	u_3/u_1	u_4/u_1
free-flow	1.013	1.027	1.011
a25-θ90-d000	1.026	1.030	0.970
a25-θ90-d150	1.033	0.938	1.022
a25-θ90-d300	0.923	0.961	0.878
a25-θ75-d000	1.078	0.861	0.895
a25-θ75-d150	1.093	1.056	1.085
a25-θ75-d300	0.973	1.088	0.903
a25-θ60-d000	1.001	1.016	1.077
a25-θ60-d150	1.019	0.995	0.945
a25-θ60-d300	1.034	1.055	0.933
a00-θ90-d150	0.984	0.311	0.352
a00-θ90-d300	0.897	1.153	0.203
a00-θ75-d150	1.039	0.398	0.479
a00-θ75-d300	0.968	1.071	0.267
a00-θ60-d150	1.090	0.500	0.315
a00-θ60-d300	1.105	1.089	0.479

Table 6.6 – Velocity measured at x_2 = 50 mm, x_3 = 200 mm, and x_4 = 350 mm, normalised by u_1 measured at x_1 = –100 mm

The small changes in velocity are imputed to the natural fluctuations or accidental errors in the measuring, hence they are not considered depending on the system configuration. For the control test, as a matter of fact, the velocity magnitude can be considered a constant without committing substantial errors in the investigated segment.

In the Figures 6.12, 6.13, 6.14, 6.15 and 6.16, all the front velocity evolutions are shown as they interact with the barrier system, grouped in diagrams by different values of *a* and *d*. Vertical bars are placed in correspondence of the second dam position.

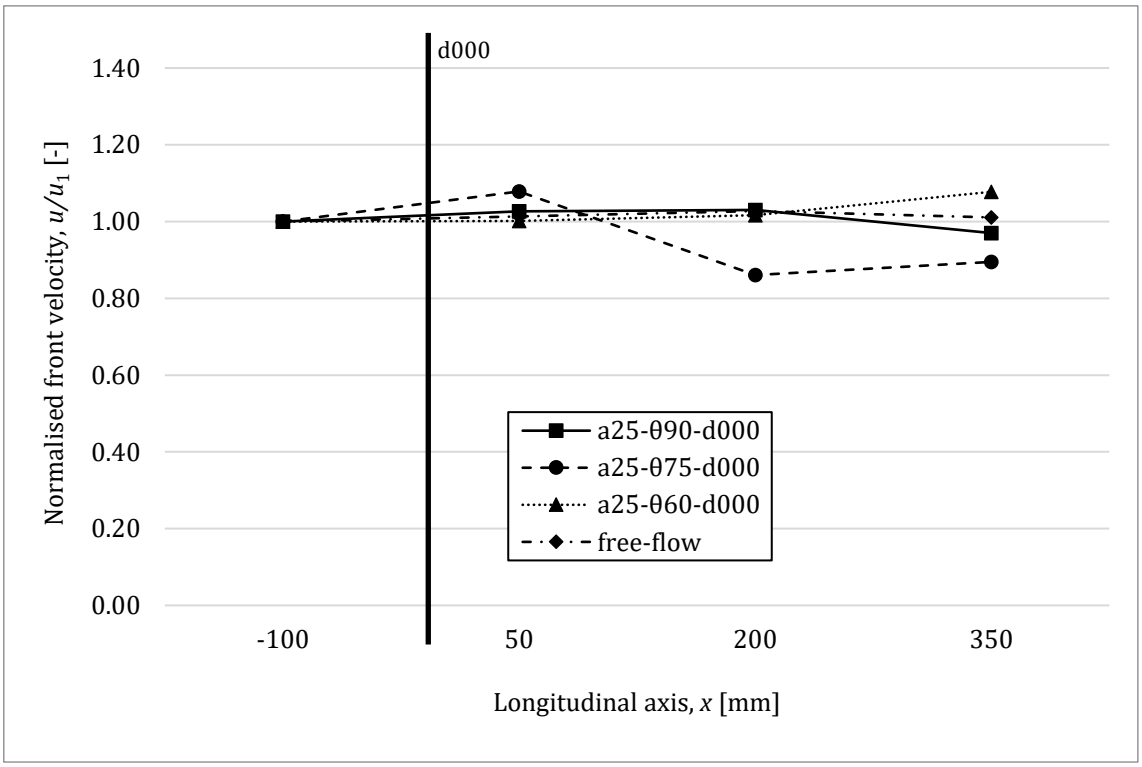

Figure 6.12 – Evolution of front velocity normalised by the initial value in the case of *a* = 25 mm and *d* = 0 mm

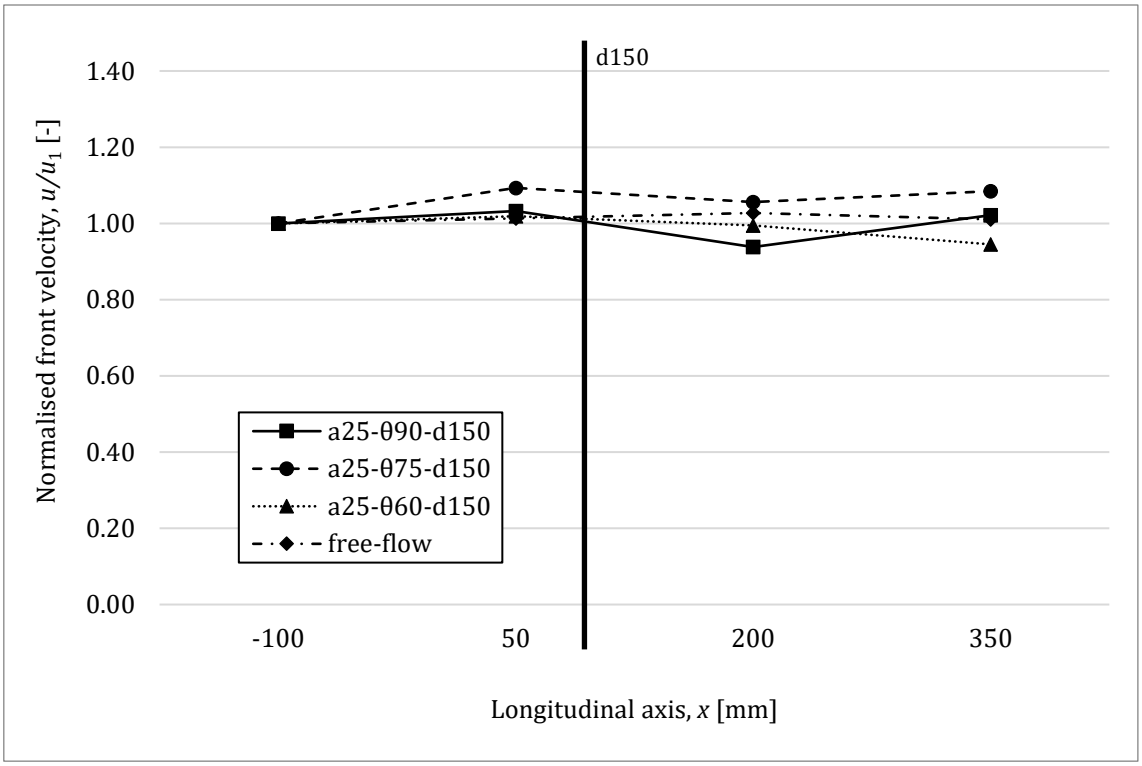

Figure 6.13 – Evolution of front velocity normalised by the initial value in the case of a = 25 mm and d = 150 mm

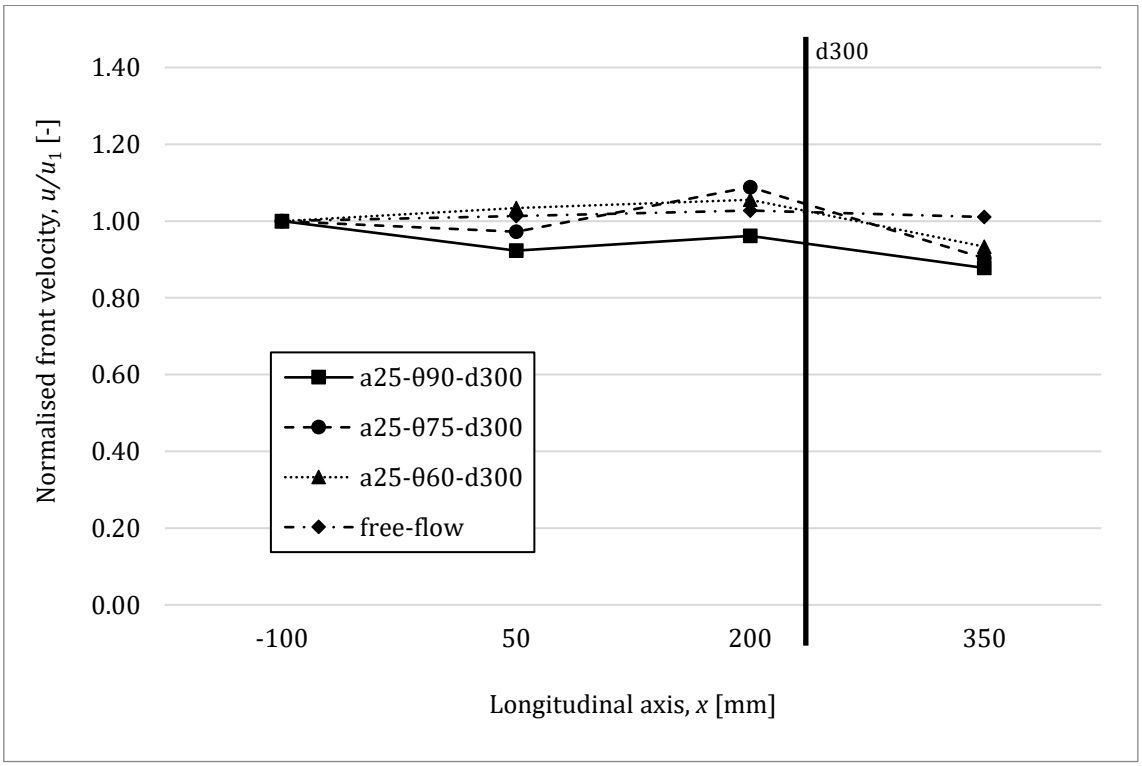

Figure 6.14 – Evolution of front velocity normalised by the initial value in the case of a = 25 mm and d = 300 mm

Since the central aperture allows the centre-line of the mass to flow down undisturbed, no matter the angle and the spacing, the configurations with a = 25 mm do not influence the front velocity. Those configurations, though, reduce the flow width of the front, generating a loss of momentum.

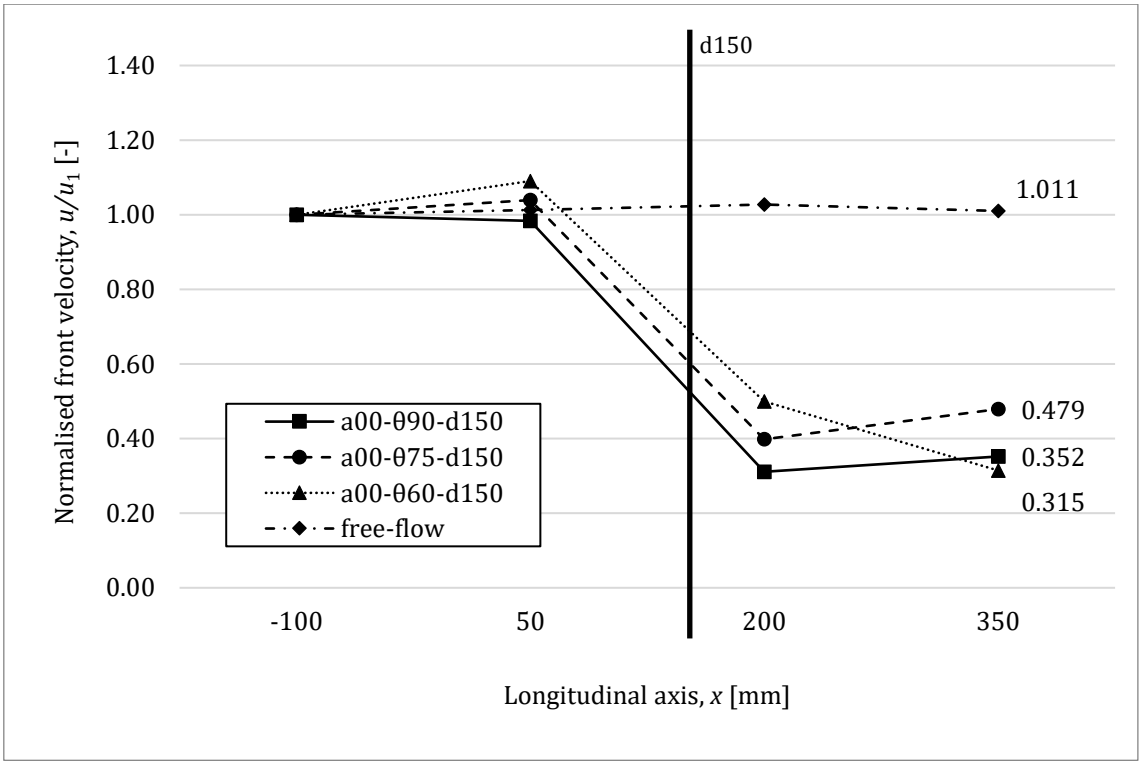

Figure 6.15 – Evolution of front velocity normalised by the initial value in the case of a = 0 mm and d = 150 mm

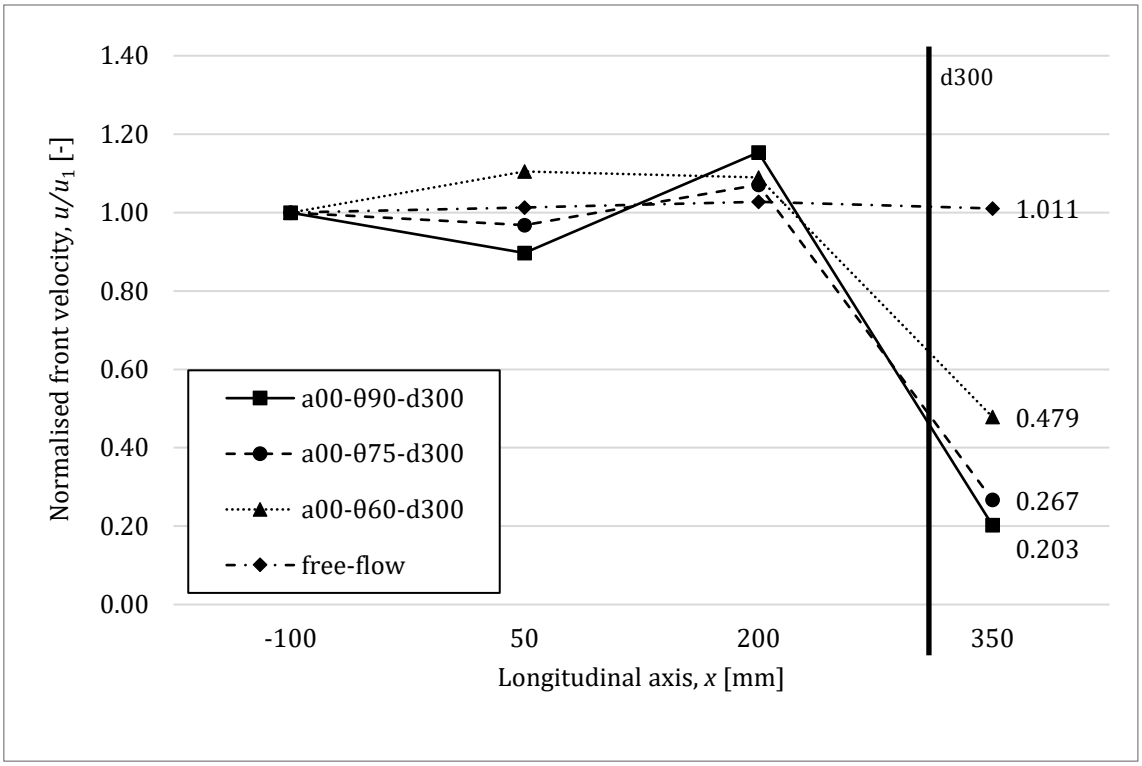

Figure 6.16 – Evolution of front velocity normalised by the initial value in the case of a = 0 mm and d = 300 mm

In case of a = 0 mm it is clearly obtained a severe reduction of front velocity, and the strongest dissipations of momentum are registered for θ = 90°.

In Figures 6.17, 6.18 and 6.19 configurations with the same deflection angle θ and a = 0 mm are highlighted.

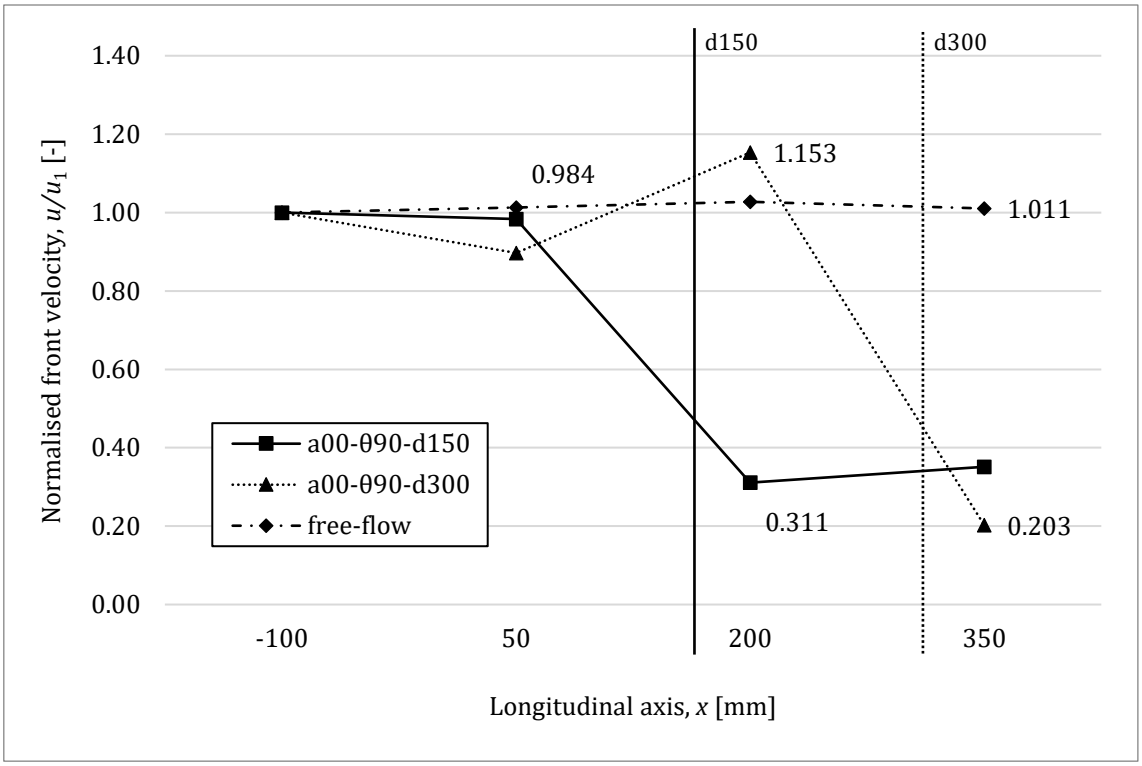

Figure 6.17 – Evolution of front velocity normalised by the initial value in the case of a = 0 mm and θ = 90°

For θ = 90°, as shown in Figure 6.17, after impacting on the second barrier at d = 150 mm, the flow front follows the deflection angle and reaches a velocity U_3 = 0.311, while it is reported a final normalised velocity U_4 = 0.203 after the impact on the second barrier at d = 300 mm. For d = 150 mm, the velocity changes from 0.984 to 0.311 after impacting the second dam, developing a change ratio U_3/U_2 = 0.316 by the dam. On the other hand, for d = 300 mm, the velocity falls from 1.153 to 0.203 after impacting the second dam, generating a change ratio U_4/U_3 = 0.176 due to the dam. At the end of the segment, the two final normalised velocities U_4 are fairly similar.

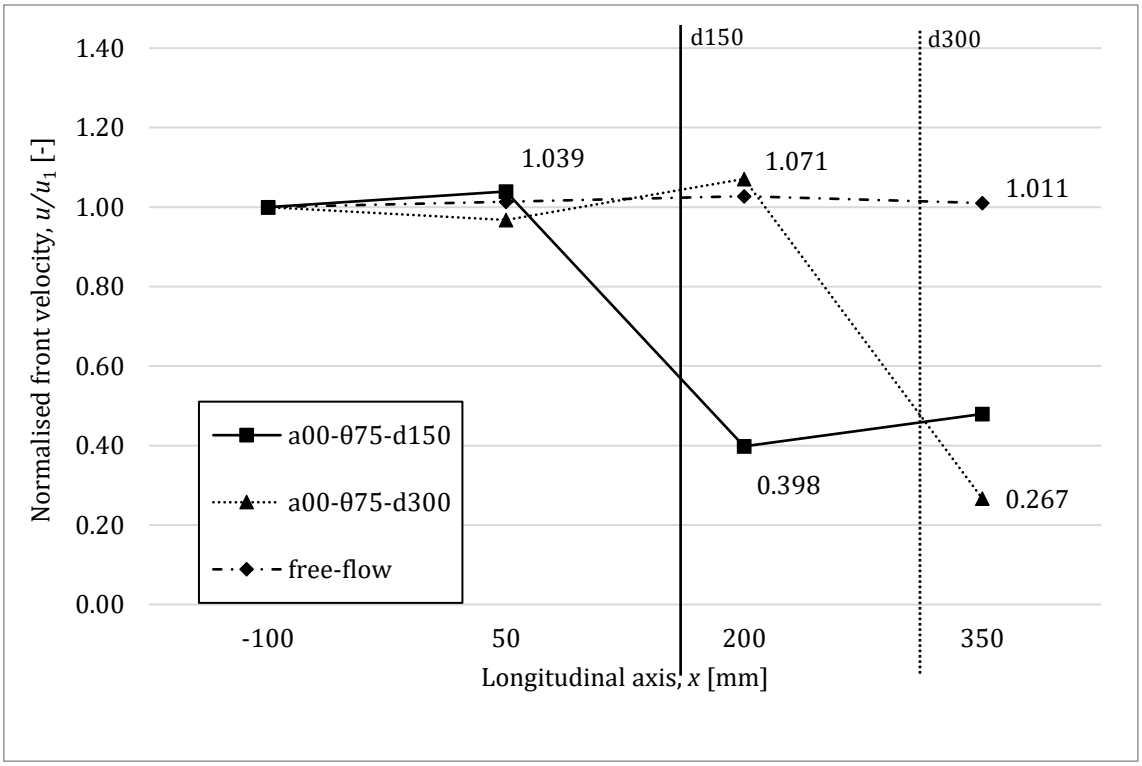

Figure 6.18 – Evolution of front velocity normalised by the initial value in the case of a = 0 mm and θ = 75°

Observing Figure 6.18, for θ = 75° and d = 150 mm the normalised velocity falls from 1.039 to 0.398 after impacting the second dam, with a change ratio U_3/U_2 = 0.383, while for d = 300 mm the velocity goes from 1.071 to 0.267, developing a change ratio U_4/U_3 = 0.249 between the values before and after the impact. The final velocities are still similar.

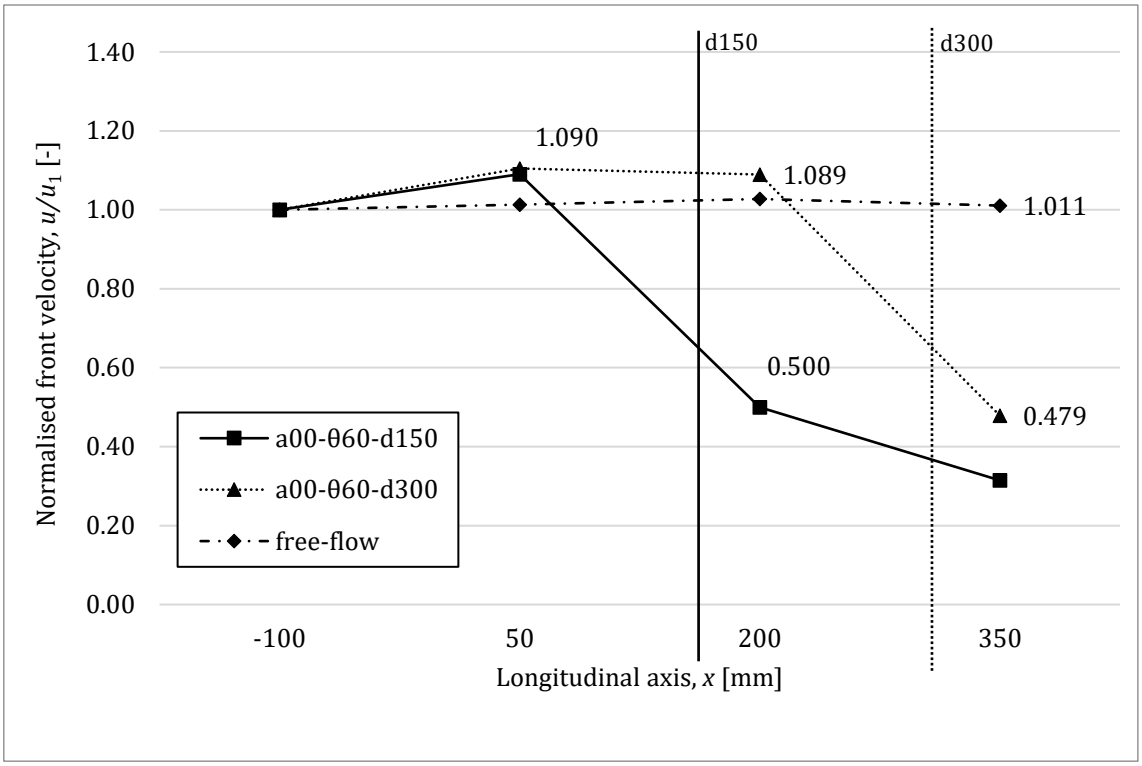

Figure 6.19 – Evolution of front velocity normalised by the initial value in the case of a = 0 mm and θ = 60°

Figure 6.19 shows that in case of for θ = 60° the slightest dissipations are observed, reaching a velocity U_3 = 0.500 when d = 150 mm, while the velocity reaches U_4 = 0.479 when d = 300 mm. Finally, for d = 150 mm the normalised velocity falls from 1.090 to 0.500 after impacting the second dam, with a change ratio U_3/U_2 = 0.458, while for d = 300 mm the velocity goes from 1.089 to 0.479 after impacting the second dam, developing a change ratio U_4/U_2 = 0.439 between the magnitudes before and after the dam. Again, the final velocities are close.

The velocity change ratio VCR by the second dam can be defined as

$$VCR = \frac{u_3}{u_2} = \frac{U_3}{U_2} \quad \text{for } d = 150 \text{ mm}$$

$$VCR = \frac{u_4}{u_3} = \frac{U_4}{U_3} \quad \text{for } d = 300 \text{ mm}$$

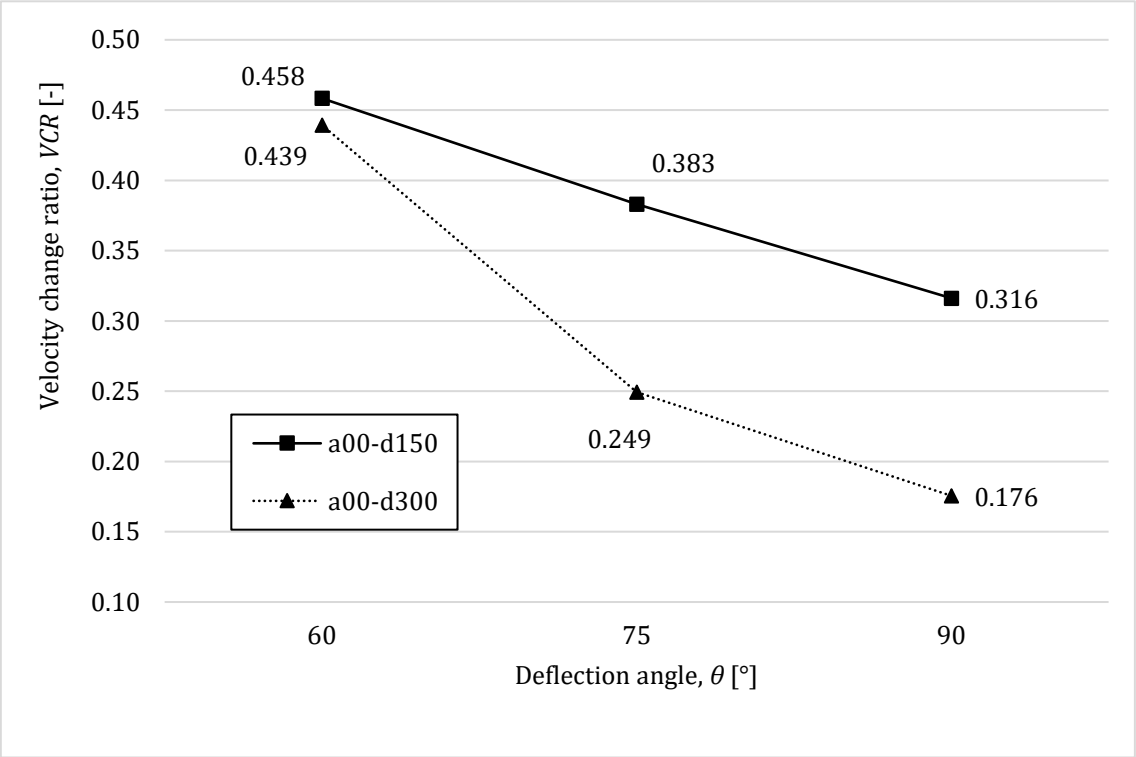

Figure 6.20 – Front velocity change ratio *VCR* by the dam, when a = 0 mm, for different deflection angles θ

Figure 6.20 evidences the influence that the deflecting angle exercises on the velocity change ratio *VCR* between the front velocities before and after the impact with the second dam of the system. The relationship between *VCR* and θ is clearly monotonically decreasing for both the series on the diagram. The graph also suggests that, with fixed deflecting angle, the larger the spacing d the lower the velocity change ratio. That is probably a coincidence, since the change ratio is a local quantity related only to a single dam, and it should be not affected by the entire system. That requires further analyses.

7. Conclusions

7.1 Retaining capacity

The retaining effectiveness of the deflecting system is estimated by evaluation of the mass entrapped upstream the obstacles. With a mean value of 0.93 kg and a maximum deviation of 0.37 kg, the retained mass results range from 0.7 kg, corresponding to 1.56 % of the total mass, to 1.3 kg, which is 2.89 %.

The survey verifies that the highest amounts of retained mass are observed when the aperture a = 0 mm. As a matter of fact, for a = 25 mm the entrapped mean value is 0.84 kg representing 1.88 % of the total mass, and for a = 0 mm the relative mean value amounting to 1.05 kg corresponds 2.33 %.

After the sand flows down, a residual thickness of material is registered at the dams. This quantity appears to be strongly affected by the deflection angle, as it decreases with θ increasing. The trend is observed for both values of a and for any spacing d. The maximum residual thickness obtained is 105 mm (a00-θ90-d300), while the minimum is 50 mm (a25-θ60-d300). The residual thickness slightly depends on the aperture as well, as for a = 0 mm all the values are above the respective ones measured for a = 25 mm.

7.2 Peak flow depth

As the flow impacts on the dam, a sudden increment of depth occurs lifting up the free surface of the flow. The observed runups range between 160 mm and 180 mm, 4.0 times the initial depth and 4.5 times, respectively. The flow depth change ratio is influenced by the spacing d and the deflection angle θ. In case of a = 25 mm, the peak depth h_{max} decreases when d increases or θ decreases. When a = 0 mm, it happens the same, except for θ = 90° which generates the maximum value of flow depth, no matter the spacing. Investigations between θ = 75° and θ = 90° may answer to this change of trend.

7.3 **Front velocity**

When there is a central aperture between the dams, the flow front is stopped by the dams at the sides, but it is free to slide in the centre. For this reason, the front velocity when a = 25 mm is not affected by the obstacles. In those cases, however, the flow width of the front is reduced to 25 mm, and that decrease indeed the flow moment and kinetic energy.

On the contrary, with a = 0 mm strong losses of front velocity occur, with the peak reduction obtained for θ = 90°. After impacting on the second barrier, the flow front follows the deflection angle and reaches a normalised velocity U_3 = 0.311 for d = 150 mm, and a normalised velocity U_4 = 0.203 for d = 300 mm.

With d = 150 mm it is observed a velocity change ratio VCR = 0.316 after the impact on the second dam, and with d = 300 mm, the change ratio is VCR = 0.176, which is even more severe.

It is also confirmed that the change ratio in velocity VCR by the second dam is a decreasing function of the deflection angle θ. Surprisingly, the second strongest loss VCR = 0.249 appears to occur for d = 300 and θ = 75°, and not for d = 150 and θ = 90° as expected. As a matter of fact, from results it appears that VCR would be also dependent on the spacing d, and that has to be better comprehended.

References

O. Hungr, D. F. VanDine, D. R. Lister (1987), Debris flow defences in British Columbia, *Geological Society of America, Reviews in Engineering Geology, Volume VII*

U. Domaas, C. B. Harbitz (1998), On avalanche runup heights on deflecting dams: centre-of-mass computations compared to observations, in: E. Hestnes, *25 Years of Snow Avalanche Research, Voss 12-16 May 1998, Proceedings,* Oslo, Norwegian Geotechnical Institute, 94-98

F. Irgens, B. Schieldrop, C. B. Harbitz, U. Domaas, R. Opsahl (1998), Simulations of dense-snow avalanches on deflecting dams, *Annals of Glaciology,* 26, 265-271

I. Herle and G. Gudehus (1999), Determination of parameters of a hypoplastic constitutive model from properties of grain assemblies, *Mechanics of Cohesive-Frictional Materials*, 4, 461-486

J. M. N. T. Gray, A. Irmer, Y. C. Tai, K. Hutter (1999), Plane and oblique shocks in shallow granular flows, *22nd International Symposium of Shock Waves, Imperial College,* London, United Kingdom, 1999 July 18-23, Paper 4550

C. B. Harbitz, U. Domaas, A. Engen (2000), Design of snow avalanche deflecting dams, *Internationales Symposion, INTERPRAEVENT 2000*, Villach, Austria, Tagungspublikation 1, 383-396

O. Hungr, S. G. Evans, M. J. Bovis, J. N. Hutchinson (2001), A review of the classification of landslides of the flow type, Geological Society of America, *Environmental and Engineering Geoscience*, Vol VII, No. 3, August 2001, pp. 221-238

T. Jóhannesson (2001), Run-up of two avalanches on deflecting dams at Flateyri, north-western Iceland, *Annals of Glaciology*, 32, 350-354

D. Issler (2003), Experimental information on the dynamics of dry-snow avalanches, in: K. Hutter, N. Kirchner (eds.), *Dynamic Response of Granular and Porous Materials under Large and Catastrophic Deformations*, Springer Berlin, 109–160

J. M. N. T. Gray, Y. C. Tai, S. Noelle (2003), Shock Waves, dead zones and particle-free regions in rapid granular free-surface flows, *Journal of Fluid Mechanics*, 491, 161-181

M. Primus, F. Naaim-Bouvet, M. Naaim, T. Faug (2004), Physical modelling of the interaction between mounds or deflecting dams and powder snow avalanches, *Cold Regions Science and Technology*, 39, 257-267

K. M. Hákonardóttir, A. J. Hogg (2005), Oblique shocks in rapid granular flows, *Physics of Fluids*, 17, 077101

J. M. N. T. Gray, X. Cui (2007), Weak strong and detached oblique shocks in gravity-driven granular free-surface flows, *Journal of Fluid Mechanics*, 579, 113-136

X. Cui, J. M. N. T. Gray, T. Jóhannesson (2007), Deflecting dams and the formation of oblique shocks in snow avalanches at Flateyri, Iceland, *Journal of Geophysical Research*, 112, F04012

J. Hubl, J. Suda, D. Proske, R. Kaina, C. Scheidl (2009), Debris flow impact estimation, *International Symposium on Water Management and Hydraulic engineering*, Ohrid, Macedonia, 2009 September 1-5, Paper A56

T. Jóhannesson, P. Gauer, D. Issler, K. Lied (2009), The design of avalanche protection dams: Recent practical and theoretical developments, Brussels, Belgium, Directorate-General for Research, Environment Directorate, European Commission, Publication EUR 23339

A. Volkwein, C. Wendeler, G. Guasti (2011), Design of flexible debris flow barriers, *Italian Journal of Engineering Geology and Enviroment*, 1093-1100

J.S.H. Kwan (2012), Supplementary technical guidance on design of rigid debris-resisting barriers, *GEO Report 270*, Geotechnical Engineering Office, Civil Engineering and Development Department, The Government of the Hong Kong S.A.R.

P. Kattel, J. Kafle, J. T. Fischer, M. Mergili, B. M. Tuladhar, S. P. Pudasaini (2018), Interaction of two-phase debris flow with obstacles, *Engineering Geology*, 242, 197-217

H. O. Pétursson, K. M. Hákonardóttir, A. Thoroddsen (2019), Use of OpenFOAM and RAMMS Avalanche to simulate the interaction of avalanches and slush flows with dams, *International symposium on Mitigative Measures against Snow Avalanches and Other Rapid Gravity Mass Flows,* Siglufjörður, Iceland, 2019 April 3-5